Entrainment Maps: A New Tool for Understanding Properties of Circadian Oscillator Models

Casey O. Diekman[1] and Amitabha Bose
Department of Mathematical Sciences,
New Jersey Institute of Technology, Newark, New Jersey

Abstract Circadian oscillators found across a variety of species are subject to periodic external light-dark forcing. Entrainment to light-dark cycles enables the circadian system to align biological functions with appropriate times of day or night. Phase response curves (PRCs) have been used for decades to gain valuable insights into entrainment; however, PRCs may not accurately describe entrainment to photoperiods with substantial amounts of both light and dark due to their reliance on a single limit cycle attractor. We have developed a new tool, called an entrainment map, that overcomes this limitation of PRCs and can assess whether, and at what phase, a circadian oscillator entrains to external forcing with any photoperiod. This is a 1-dimensional map that we construct for 3 different mathematical models of circadian clocks. Using the map, we are able to determine conditions for existence and stability of phase-locked solutions. In addition, we consider the dependence on various parameters such as the photoperiod and intensity of the external light as well as the mismatch in intrinsic oscillator frequency with the light-dark cycle. We show that the entrainment map yields more accurate predictions for phase locking than methods based on the PRC. The map is also ideally suited to calculate the amount of time required to achieve entrainment as a function of initial conditions and the bifurcations of stable and unstable periodic solutions that lead to loss of entrainment.

Keywords entrainment, iterated map, limit cycle, mathematical modeling, periodically forced oscillator, phase response curve, photoperiod, Poincaré section

The ability of circadian oscillators to entrain to daily cycles of light and temperature has been called both the most important and the most misunderstood property of circadian rhythmicity (Johnson et al., 2003). Entrainment implies that an endogenous oscillator has matched its period to that of an external periodic forcing and has established a stable phase relationship with the forcing signal. The process of circadian entrainment has been studied extensively using tools from dynamical systems and oscillator theory (Ananthasubramaniam et al., 2014; Bagheri et al., 2008; Bordyugov et al., 2013a; Gu et al., 2012, 2013; Indic et al., 2006; Johnson et al., 2003; Leise and Siegelmann, 2006; Leloup and Goldbeter, 2013; Ramkisoensing et al., 2014; Rand et al., 2004; Roenneberg et al., 2003; Serkh and Forger, 2014; Woller et al., 2014). Perhaps the most commonly used method relies on phase response curves (PRCs) that measure the change in the phase of an endogenous limit cycle oscillation (typically in constant darkness or DD) induced by a perturbation (typically a light pulse) as a function of the phase at which the perturbation is applied (Johnson, 1999). Alternatively, one

1. To whom all correspondence should be addressed: Casey O. Diekman, Department of Mathematical Sciences, New Jersey Institute of Technology, Newark, NJ 07102, USA; e-mail: diekman@njit.edu.

JOURNAL OF BIOLOGICAL RHYTHMS, Vol. 31 No. 6, December 2016 598–616
DOI: 10.1177/0748730416662965

could perturb an oscillator in constant light (LL) with dark pulses. Such PRCs can be constructed for light or dark pulses of arbitrary strength and duration. However, for a PRC to accurately predict properties of entrainment to periodic light or dark pulses, the perturbations must be weak or brief enough that the oscillator relaxes back to the DD or LL limit cycle attractor before the next pulse arrives. Since circadian oscillators are naturally subject to forcing in which the light duration is several hours followed by several hours of darkness, the PRC may not be ideally suited to accurately determine entrainment in this context. In fact, we show that PRCs do not accurately predict the phase of entrainment in 3 different mathematical models of circadian clocks that are subjected to photoperiods with substantial amounts of both light and dark, such as 12-h:12-h light-dark (12:12 LD) cycles. For these LD cycles, the entrained solution is best thought of as a combination of 2 limit cycle attractors (i.e., the DD and LL limit cycles), rather than as a perturbation of a single limit cycle attractor (Peterson, 1980).

In this paper, we introduce a new tool, a 1-dimensional *entrainment map*, which is not based on perturbing the DD or LL oscillator. Instead, the map uses information on how both the 12-h light period and the 12-h dark period affect cycle duration as a function of the time elapsed since the lights last turned on. We show that the stable fixed point of the map corresponds to a stable LD-entrained solution. Properties of the entrained solution, such as the range of entrainment as a function of parameters or the speed with which entrainment occurs, are then inferred from properties of the map. We demonstrate that the map accurately predicts the phase of entrainment independent of the photoperiod across a variety of different models. Our findings are consistent with previous results in the literature (Bordyugov et al., 2015; Granada et al., 2013) and provide a new method for studying high-dimensional circadian models that are difficult to analyze mathematically.

The entrainment map is an example of an iterated map, a class of dynamical systems in which time is treated as discrete rather than continuous (Strogatz, 1994; Wu and Rul'kov, 1993). One-dimensional iterated maps have the form

$$x_{n+1} = \Pi(x_n), \tag{1}$$

where Π is a function that maps values from an interval back into that interval. Maps can be used as models of natural phenomena where time is inherently discrete or as tools for analyzing continuous-time models consisting of ordinary differential equations (ODEs). The entrainment map we develop is an example of the latter and, in principle, can be constructed for any of the myriad ODE models of circadian clocks in the literature, from detailed models of molecular clocks in a variety of species to phenomenological models of human circadian rhythms (Bordyugov et al., 2013b; Forger et al., 2007; Gonze, 2011; Roenneberg et al., 2008). The maps live in lower dimensional spaces than the original systems, which facilitates geometric visualization and the understanding of complicated dynamics. For example, many circadian ODE models exhibit limit cycle oscillations. These periodic solutions correspond to fixed points of the maps. Determining properties of these steady-state solutions, such as stability, is much easier for fixed points than for limit cycles. Furthermore, solution trajectories of maps are found by iterating the function Π to obtain a sequence of x values that dictate the behavior of solutions of the map and, as a result, the corresponding ODE (Hirsch et al., 2013).

We construct entrainment maps for circadian oscillators under forcing by a periodic light-dark cycle. For this map, the variable x_n tracks the number of hours that have passed in the nth light-dark cycle between the lights turning on (defined as $x = 0$) and the oscillator reaching a certain location in phase space. Both x and $\Pi(x)$ take values between 0 and 24, where $x = 0$ and $x = 24$ are equivalent. Thus, Π maps a circle onto itself and is referred to as a *circle map*. The theory of circle maps is well-developed and has been applied extensively to study cardiac rhythms and other types of biological oscillators (Glass, 1991; Keener and Glass, 1984; Winfree, 2001). More generally, the search for an entrained solution is an example of a classic problem in which an oscillator is forced by an external periodic input. Much prior theoretical work has been done in the context of circadian oscillators (Bordyugov et al., 2015; Roenneberg et al., 2003, 2010a). What is common to all of these studies, as well as ours, is that there exists a range of parameters over which the period of the oscillator becomes equal to that of the forcing, and stable one-to-one entrainment occurs.

In this paper, we focus on 3 distinct circadian oscillator models of different complexity. The first is the Novak-Tyson (NT) model of the *Drosophila* molecular clock (Tyson et al., 1999). This is a 2-dimensional model for which we provide a detailed derivation of the entrainment map. The other two models we consider are the 3-dimensional Gonze model (Gonze et al., 2005) and the 180-dimensional Kim-Forger model (Kim and Forger, 2012) of the mammalian molecular clock. For all of these models, we demonstrate that the map accurately predicts the stable entrained phase relative to the underlying light-dark forcing. Additionally, we show that the map enables us to characterize, across different models, how properties such as the range of entrainment depend on parameters associated with the intrinsic oscillator and the external forcing. In this sense, the map reveals

certain universal properties about how different circadian models respond to changes in parameters that are common to all models, such as the speed of the intrinsic oscillator, light intensity, and photoperiod. In turn, this provides insights and the ability to make predictions about higher dimensional models that are not so easily gained through direct simulations.

MODEL AND METHODS

In this section we introduce the circadian clock models that we shall use in our study and the 1-dimensional map that we have developed to analyze entrainment properties of such models.

The Novak-Tyson Model

The NT model (Novak and Tyson, 2008; Tyson et al., 1999) for the molecular circadian clock in the fruit fly *Drosophila* contains 2 state variables representing mRNA concentration (M) and protein (P) concentration:

$$\begin{aligned} \frac{1}{\phi}\frac{dP}{dt} &= M-(k_D+k_L f(t))P-k_f\frac{P}{0.1+P+2P^2} \\ \frac{1}{\phi}\frac{dM}{dt} &= \varepsilon\left(\frac{1}{1+P^4}-M\right) \end{aligned}, \quad (2)$$

where all parameters are positive. The P variable represents 2 proteins (PER and TIM) that form a heterodimer and create a negative feedback loop by inhibiting transcription of their own genes. The parameter ε is taken to be small, which creates a separation of time scales between the P and M variables. The parameter ϕ governs the rate of flow of trajectories in the phase plane and will directly affect the period of any solutions we find. The parameter k_D is the baseline protein degradation rate during darkness. In *Drosophila*, light is known to increase degradation of TIM; k_L is the added degradation rate due to light. The parameter k_f captures the extent of positive feedback due to stabilization of the protein after dimerization. The function $f(t)$ describes the light stimulus. In complete darkness, $f(t)\equiv 0$. In complete light, $f(t)\equiv 1$. When the model is subjected to a periodic photoperiod, $f(t)$ is chosen to be a smooth cut-off version of a periodic step function that takes on the value 0 during darkness and 1 during light.

Consider first the situation of either constant darkness $f(t)\equiv 0$, or constant light, $f(t)\equiv 1$. In each case, the nullclines consist of the set of points where the right-hand sides of the equations in Equation (2) equal 0. In particular, we define P-nullclines for each case together with a common M-nullcline.

$$\begin{aligned} \mathcal{N}_{P_D}: &\quad M = k_D P + k_f\frac{P}{0.1+P+2P^2} \\ \mathcal{N}_{P_L}: &\quad M = (k_D+k_L)P + k_f\frac{P}{0.1+P+2P^2} \\ \mathcal{N}_M: &\quad M = \frac{1}{1+P^4} \end{aligned}. \quad (3)$$

Both $\mathcal{N}_{P_D}$ and $\mathcal{N}_{P_L}$ form cubic shaped curves in the $P-M$ phase plane. We sometimes use the notation $\mathcal{N}_P$ to refer to the P-nullcline when it does not matter whether we are referring to dark or light. The curve $\mathcal{N}_M$ is qualitatively sigmoidal shaped. Depending on where the P and M nullclines intersect, the ensuing fixed point(s) may be stable or unstable. Any intersection that occurs on the left or right branches of P-nullclines are stable, while those that occur on the middle branch will be unstable provided that ε and k_D are not too large. The standard set of parameters that we use for a single cell produces an unstable fixed point along the middle branch. In either constant darkness or constant light, it is straightforward to use dynamical systems methods to prove the existence of a stable limit cycle (periodic orbit) solution, as discussed in the Results section.

The Gonze Model and the Kim-Forger Model

We also consider 2 different models of the molecular circadian clock in mammals. The Gonze model (Gonze et al., 2005) is a modified version of the Goodwin oscillator (Goodwin, 1965) describing the core negative feedback loop of the circadian cock. There are 3 state variables that represent concentrations of mRNA (M), protein (P_1), and protein in its active form (P_2) of a clock gene such as *Per* or *Cry*:

$$\begin{aligned} \frac{1}{\phi}\frac{dM}{dt} &= (\nu_D+\nu_L f(t))\frac{k_1^4}{k_1^4+P_2^4}-\nu_2\frac{M}{k_2+M} \\ \frac{1}{\phi}\frac{dP_1}{dt} &= k_3 M-\nu_4\frac{P_1}{k_4+P_1} \\ \frac{1}{\phi}\frac{dP_2}{dt} &= k_5 P_1-\nu_6\frac{P_2}{k_6+P_2} \end{aligned}. \quad (4)$$

Specifically, P_2 is the nuclear form of PER/CRY that inhibits transcription of the clock gene. In mammals, light is known to increase the transcription rate of *Per1* and *Per2* (Golombek and Rosenstein, 2010); thus, we have included the LD forcing in the first term of the dM/dt equation. The following parameter values were used: $\nu_D=0.7$, $\nu_L=0.1$, $k_1=1$, $\nu_2=0.35$, $k_2=1$, $k_3=0.7$, $\nu_4=0.35$, $k_4=1$, $k_5=0.7$, $\nu_6=0.35$, and $k_6=1$.

The Kim-Forger model contains the core negative feedback loop as well as additional secondary

feedback loops. The model has 180 state variables representing nuclear and cytoplasmic concentrations of mRNA and protein products for several clock genes including *Per1, Per2, Cry1, Cry2, Bmal, Npas2*, and *Rev-erb*, as well as other regulatory elements. For a detailed description of the full model, see Forger and Peskin (2003) and Kim and Forger (2012). Here we only show the differential equations for the 2 state variables that receive LD forcing, which are *Per1* and *Per2* mRNA in the nucleus ($MnPo$ and $MnPt$), and the state variable that we will use to define the entrainment map for this model, which is BMAL protein in the cytoplasm (B):

$$\begin{aligned}\frac{1}{\phi}\frac{d(MnPo)}{dt} &= (trPo_D + tr_L f(t))G \\ &\quad -(tmc)(MnPo) - (umPo)(MnPo) \\ \frac{1}{\phi}\frac{d(MnPt)}{dt} &= (trPt_D + tr_L f(t))G \\ &\quad -(tmc)(MnPt) - (umPt)(MnPt) \\ \frac{1}{\phi}\frac{dB}{dt} &= (tlb)(McB) - (cbin)(Cl)B \\ &\quad +(uncbin)(BC) - (ub)B\end{aligned} \quad , \qquad (5)$$

where G, McB, Cl, and BC are state variables representing the probability of the E-box promoter being activated, *Bmal* mRNA and CLOCK/NPAS2 protein concentrations in the cytoplasm, and the concentration of unphosphorylated BMAL-CLOCK/NPAS2. The parameters $trPo_D$ and $trPt_D$ are basal transcription rate constants in darkness, tr_L is additional transcription due to light, $umPo$ and $umPt$ are degradation rate constants, and tmc is the rate constant for folding and nuclear export of mRNA. Finally, the parameters tlb, ub, $cbin$, and $uncbin$ are rate constants for BMAL translation, BMAL degradation, and binding and unbinding of BMAL to CLOCK/NPAS2. We used the parameter values given in Kim and Forger (2012), with $trPo_D = 25.9201$, $trPt_D = 44.854$, and $tr_L = 10$.

For all 3 of these models, we will show via simulation that the 1-dimensional entrainment map yields accurate predictions for the phase of entrainment.

Effects of Sensory Input: Light and Darkness

We shall be interested in the response to 3 different scenarios: constant darkness, constant light, and periodic switching between the two with a prescribed photoperiod. We will show that over a wide range of parameters, the models produce stable periodic solutions in constant darkness, referred to as DD, or in constant light, denoted LL. We denote the "free-running" period of the DD oscillator as τ. In the case of periodic forcing, we follow a protocol that is often used in experiments. Namely, we will study the entrainment of oscillators to a periodic signal that models a photoperiod of a 24-h cycle consisting of an N hour "light" interval (L) followed by a 24-N hour "dark" interval (D). When an oscillator is subjected to a light-dark photoperiod (LD), depending on parameters, it may entrain to the 24-h forcing. By *entrain* we mean that the solution is periodic and that it has a period of 24 h. If these conditions are met, we call the ensuing periodic solution an *LD-entrained solution*.

To consider an oscillator subjected to periodic forcing of N hours of light followed by $24-N$ hours of darkness, we allow $f(t)$ to vary periodically between 0 and 1. In our simulations, $f(t)$ is a rectangular wave with instantaneous transitions. When analyzing the periodically forced system, we consider $f(t)$ to be a smooth approximation of a rectangular wave.

The Entrainment Map $\Pi(x)$

The entrainment map $\Pi(x)$ is the primary tool we will use to understand the properties and consequences of phase-locking. To define $\Pi(x)$, we choose a Poincaré section $\mathcal{P}$ as an $n-1$ dimensional hyperplane that intersects a point on the LD cycle. To define a hyperplane, we only need to specify the value of 1 of the variables and the direction of the flow as it crosses the hyperplane. For example, in the 2-dimensional NT model, $\mathcal{P}$ is a 1-dimensional line segment that intersects the LD-entrained solution chosen along the left branch of $\mathcal{N}_P$ at $M = 0.44$ where $dM/dt > 0$. This is a natural location to place $\mathcal{P}$ since the flow forces trajectories to enter a neighborhood of that branch. We note that the method still works if we choose $\mathcal{P}$ to lie along a different portion of the LD cycle, for example, away from the left branch, as discussed in the Supplementary Material, Section R2. In the Gonze and Kim-Forger models, there is no natural location to choose for the Poincaré section. We choose the section in these cases by specifying a variable that does not receive the light-dark forcing. For the 3-dimensional Gonze model, $\mathcal{P}$ is a 2-dimensional hyperplane chosen at $P_1 = 0.35$ where $dP_1/dt > 0$. For the 180-dimensional Kim-Forger model, $\mathcal{P}$ is a 179-dimensional hyperplane chosen at $B = 20$ where $dB/dt > 0$. Assume that the oscillator has an initial condition lying on the Poincaré section. We define x to be the amount of time that has passed since the beginning of the most recent LD cycle. When the trajectory is again on $\mathcal{P}$, we define the map $\Pi(x)$ to be the amount of time that has passed since the onset of the most recent LD cycle. The domain and range of $\Pi(x)$ are the set $[0, 24]$. The domain is considered to be periodic, where $x = 0$ and $x = 24$ are equivalent. The Poincaré map relates the value of x at one cycle to its value at the next; $x_{j+1} = \Pi(x_j)$ for

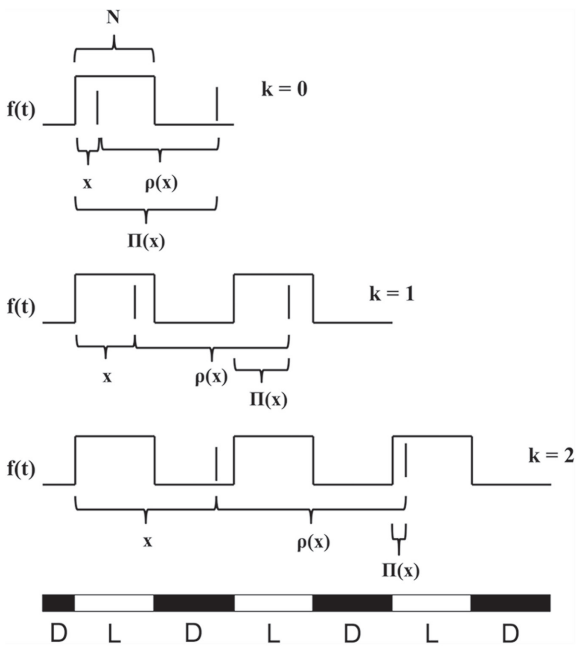

Figure 1. Schematic that defines x, $\rho(x)$, and $\Pi(x)$ in various cases. In each panel, the solid vertical lines denote 2 consecutive moments in time when the oscillator crosses the Poincaré section $\mathcal{P}$. The square wave denotes $f(t)$, which varies between 0 and 1, and the LD photoperiod is shown at the bottom of the figure. The time x is measured as the distance in time from the start of the first light pulse (when $f(t)$ increases to 1) to the first crossing of $\mathcal{P}$, and $\rho(x)$ is the distance in time between crossings of $\mathcal{P}$. The value $\Pi(x)$ measures the distance in time from the start of the most recent onset of lights to the next crossing of $\mathcal{P}$. The 3 panels shown correspond to the 3 possible scenarios that arise in defining the entrainment map.

$j \geq 0$. Unless otherwise noted, we limit our discussion of the properties of the map to parameter sets where both the LL and DD limit cycles exist. Details on how we conducted the numerical simulations to construct the map are provided in the Supplementary Material, Section M1.

The map $\Pi(x)$ can be decomposed in the following way. Define a return map $\rho(x)$ that measures the time a trajectory starting on $\mathcal{P}$, x hours into an LD cycle, takes to return to $\mathcal{P}$. Then $\Pi(x) = \rho(x) + x \bmod 24$. Because of the mod operation, it is not readily clear whether the trajectory returns to $\mathcal{P}$ in the same LD cycle in which it started or in a subsequent one. To clarify this point, note that if $\rho(x) < 24 - x$, the trajectory will return back to $\mathcal{P}$ within the same LD cycle in which it started. Thus, $\Pi(x) = \rho(x) + x$. If $24 - x < \rho(x) < 48 - x$, then the trajectory returns in the next LD cycle and $\Pi(x) = \rho(x) + x - 24$. In general, we can write $24k < \rho(x) + x < 24(k+1)$, for $k = 0, 1, 2, \ldots$ and $\Pi(x) = \rho(x) + x - 24k$. The case $k = 0$ corresponds to the trajectory returning to P in the same LD cycle it started in, $k = 1$ in the next cycle, $k = 2$ in the subsequent cycle, and so on. See Figure 1 for an illustration.

The map $\rho(x)$ measures the time it takes a trajectory leaving $\mathcal{P}$ to return to it. It has a periodic domain $[0, 24]$, and its range lies in the set of positive numbers. It has several generic properties: $\rho(x)$ is continuous (since the forced vector field of Equation (2) is smooth), $\rho(x)$ is periodic at its endpoints $\rho(0^+) = \rho(24^-)$ (since the domain is periodic), and $\rho(x)$ is decreasing on a subinterval of its domain (as shown in the Results section).

A stable fixed point of the map $\Pi(x)$, denoted x_s, corresponds to a one-to-one entrained solution and determines the phase of locking. A stable fixed point satisfies 2 conditions, $x_s = \Pi(x_s)$ and $|\Pi'(x_s)| < 1$. Both conditions can be checked by plotting the map and determining whether and with what slope the graph intersects the diagonal. When a stable, phase-locked solution exists, the map $\Pi(x)$ is ideally suited to calculate the time to approach the stable solution starting from any initial condition. If x_s is a stable fixed point of the map and $\{x_j\}$ is a sequence of iterates of the map, we say that the solution is entrained if there exists m, such that for all $j \geq m$, $|x_s - x_j| < 0.5$. Given an initial condition x_0, we use the map to determine m and thereby determine the time to entrainment. We will show by comparison to direct simulations of the full system that this method is quite accurate.

There is a considerable amount of flexibility in how the Poincaré section is chosen. This is because of a basic theoretical result of smooth differential equations: namely, that solution trajectories depend continuously on initial conditions. To build the map $\Pi(x)$, for each x, we start with an initial condition that lies on the intersection of $\mathcal{P}$ and the LD-entrained solution (e.g., in the Gonze model at the value $M = 0.21$, $P_1 = 0.35$, and $P_2 = 1.73$). Because the value of x is not necessarily the fixed point x_s, the ensuing trajectory is not the entrained solution. But the theory of smooth dynamical systems guarantees that the solution trajectory will lie close to the LD-entrained solution for a finite amount of time. The terms close and finite can be made mathematically precise, but for our purposes it is enough to guarantee that the trajectory again crosses $\mathcal{P}$ in a neighborhood of the crossing point of the entrained solution. This basic theoretical fact is what allows the entrainment map to be constructed for high-dimensional models for which the LD-entrained solution has first been numerically computed. Different choices of the Poincaré section will lead to different entrainment maps. But for any choice, the ensuing LD-entrained solutions will all have the same phase of entrainment, as discussed in the Supplementary Material, Section R2.

The entrainment map is defined by setting $x = 0$ as the reference phase with respect to the onset of lights in a 24-h light-dark cycle. This is in contrast to

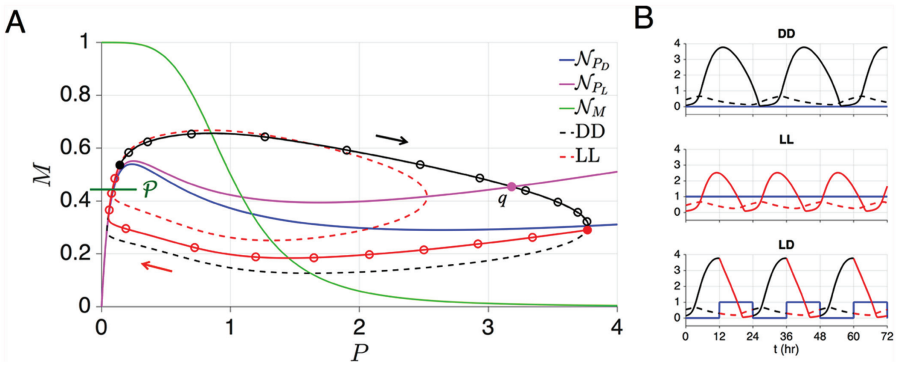

Figure 2. (A) The DD (dashed black), LL (dashed red) and LD (solid red-black) solutions of the NT model are shown in the phase plane. The LD-entrained solution overlaps the DD oscillator's trajectory during darkness (black) and then deviates from it near $P = 4$ when the lights turn on (red). Trajectories move clockwise in the plane. Open circles denote hourly intervals. The green horizontal line segment is $\mathcal{P}$. The point q is the intersection of the LD-entrained trajectory with $\mathcal{N}_{P_L}$ and is referred to in the Supplementary Material, Section R1. (B) Time courses of the P (solid) and M (dashed) variables. The free-running period of the DD oscillator ($f(t) \equiv 0$ [blue line], top trace) is longer than that of the LL oscillator ($f(t) \equiv 1$, middle trace). Entrainment to a 24-h periodic 12:12 forcing $f(t)$ (bottom trace) results in an LD-entrained oscillation.

PRC-based methods, where the reference phase is typically assigned to a point along the DD oscillator. Although it may not seem that assigning the reference phase to a point on the underlying light-dark forcing instead of DD or LL makes much of a difference, we will show that doing so allows us to use information from the DD, LL, and LD-entrained solutions to construct the map. Additionally, the entrainment map allows the light pulse (or the dark pulse) to be split up so that it appropriately represents the relationship of the oscillator to the ongoing light-dark cycle and not just as a single pulse at a predetermined phase as in a PRC. As a result, we will show that for all the models we tested, the map ends up yielding a more accurate prediction about phase locking than the PRC.

RESULTS

We begin by analyzing the NT model. Many of the details of the phase plane analysis can be found in the Supplementary Material. We then turn to the Gonze and Kim-Forger models and show that the entrainment map also works well in these higher-dimensional settings.

LD-Entrained Oscillations in the Novak-Tyson Model

When $f(t) \equiv 0$, Equation (2) produces a limit cycle corresponding to a DD oscillator (black dashed curve in Fig. 2A). This stable limit cycle exists due a simple application of the Poincaré-Bendixson theorem. Namely, one can build a bounded, positively invariant region that surrounds the single fixed point that lies on the middle branch of $\mathcal{N}_M$. Since this fixed point is unique and unstable, the Poincaré-Bendixson ensures the existence of a stable limit cycle. When $f(t) \equiv 1$, the P-nullcline shifts up in phase space, but the fixed point remains on the middle branch. Again the Poincaré-Bendixson theorem applies, proving the existence of the LL limit cycle (dashed red curve in Fig. 2A). Note that the DD limit cycle has a larger amplitude in the P direction. This is a consequence of the difference in the P-nullcline between the DD and LL cases. Also note that the 2 limit cycles share a common fast-slow structure that allows them to largely overlap near the left branch of $\mathcal{N}_P$. Indeed, as $\varepsilon \to 0$, Equation (2) becomes singularly perturbed and portions of the LL and DD trajectories would lie on the left and right branches of $\mathcal{N}_P$. For any ϕ, the period of the LL limit cycle is less than that of the DD limit cycle (the opposite is true for the Gonze and Kim-Forger models, as discussed in the section on higher dimensional models). This is a result of the faster dynamics in the LL case due to $\mathcal{N}_{P_L}$ being higher in the phase space than $\mathcal{N}_{P_D}$.

In the presence of light-dark forcing, the ensuing trajectory spends its time in phase space approaching the DD cycle during darkness and the LL cycle during light. This idea was noted in earlier work by Peterson (1980) (Johnson et al., 2003; Pittendrigh, 1981). In some sense, the trajectory uses the stable structure of the DD and LL limit cycles to transiently approach the appropriate one during relevant time intervals. For this planar model, this back and forth serves to bound where in phase space the trajectory can lie at any moment in time. The LD-entrained solution is shown in Figure 2A. Note that the entrained solution tracks the DD limit cycle for a

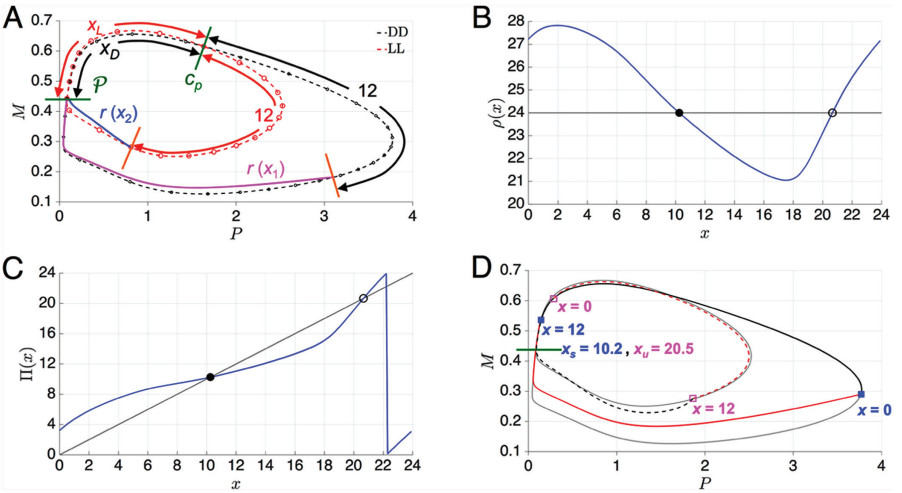

Figure 3. (A) DD (dashed black) and LL (dashed red) limit cycles with open circles indicating hourly intervals starting at $\mathcal{P}$. c_p is an intersection point of these 2 limit cycles. Times along the DD and LL limit cycles between $\mathcal{P}$ and c_p are indicated as x_D and x_L. The orange lines are located 12 h in time along the DD and LL limit cycles from the point c_p. The times $r(x_1) = 8.16$ h and $r(x_2) = 2.74$ h are numerically computed as the remaining time it takes the respective trajectories (magenta and blue) to return to $\mathcal{P}$. (B) Numerically computed $\rho(x)$. Solid and open dots depict x_s and x_u. (C) Numerically computed $\Pi(x)$. Solid and open dots depict crossings with the diagonal and correspond to the stable and unstable phase locked solutions x_s and x_u. (D) Stable (solid) and unstable (dashed) LD limit cycles corresponding to x_s and x_u. The LL (light gray, smaller amplitude) and DD (light gray, larger amplitude) solutions are shown for comparison.

portion of its trajectory and then deviates from it near $P = 3.7$. From that point, the trajectory is attracted toward the LL limit cycle, although it reaches the left branch of the P-nullcline prior to entering a neighborhood of the LL cycle. This is because the rate of attraction to the LL limit cycle is not overly large. Open circles along the LD-entrained solution denote hourly intervals. Figure 2B shows time traces of the DD, LL, and LD-entrained solutions. The latter additionally shows the relationship of the entrained solution to the light-dark pulse. For the parameters used in the simulation, the peak value of M happens to occur near the beginning of the dark period. The entrainment map will help to explain why this is the case.

Let us consider a specific set of parameters referred to as the canonical set for the NT model ($\phi = 2.1$, $k_D = 0.05$, $k_L = 0.05$, $k_f = 1$, $\varepsilon = 0.05$ and a 12:12 photoperiod). Figure 3A shows an annotated phase plane of the LL and DD cycles for this set of parameters. On the respective cycles, solid dots depict hourly intervals. The total length of time of the LL cycle is 21.64 h, and that of the DD cycle is 28.9 h. The 2 cycles effectively overlap along the left branch of $\mathcal{N}_P$. They also intersect near $P = 1.5$, $M = 0.65$. Call this point c_p. To facilitate the construction of $\Pi(x)$, let us first consider $\rho(x)$ and explain why it has an interval of points on which it is decreasing. Let x_L be the time it takes a trajectory to evolve along the LL cycle from $\mathcal{P}$ to c_p and x_D the time along DD between these 2 objects. For the case of $\phi = 2.1$, $x_L = 7$ and $x_D = 6.3$. Define $x_1 = 12 - x_L$ and $x_2 = 24 - x_D$.

Let us consider the trajectory that has initial condition x_1. This trajectory evolves along the LL cycle for x_L until it reaches c_p. At this point, the lights switch off and the trajectory now must follow the DD cycle for 12 h. The length of time of the DD cycle between c_p and $\mathcal{P}$ is 22.6 h. Thus, when the lights turn back on, the trajectory is very far from $\mathcal{P}$. In contrast, the trajectory with initial condition x_2 travels for x_D hours on DD to c_p. From here it travels 12 h on the LL cycle. The length of time on LL from c_p to $\mathcal{P}$ is 14.6 h. Thus, after 12 h on LL, the trajectory is very close to $\mathcal{P}$. If $r(x_i)$ denotes the remaining time for each trajectory to reach $\mathcal{P}$, it is clear that $r(x_1) > r(x_2)$. Given that x_L is close to x_D, it follows that $\rho(x_1) > \rho(x_2)$. The continuity of $\rho(x)$ then implies there must be a subinterval of (x_1, x_2) on which $\rho(x)$ is decreasing. Note that the actual interval on which $\rho(x)$ is decreasing may in fact contain (x_1, x_2) rather than be contained in it. Because of periodicity, $\rho(x)$ must also be increasing over a different interval(s). Figure 3B shows $\rho(x)$ for the case $\phi = 2.1$. Note that the curve is qualitatively a cubic with a single interval over which it is decreasing. This interval contains (x_1, x_2). Since $\rho(x)$ is continuous on a closed interval, it attains its maximum and minimum values. It is fairly easy to get a bound on these values. The upper bound is attained near x_1 and is obtained by taking the LL cycle from $\mathcal{P}$ to c_p and the DD cycle from c_p back to $\mathcal{P}$. This yields a time of 29.6 h. The lower bound occurs near x_2 and is obtained by taking DD from P to c_p, then LL back to $\mathcal{P}$, yielding a time of 20.9 h. This yields a bound on $d\rho(x)/dx$ on

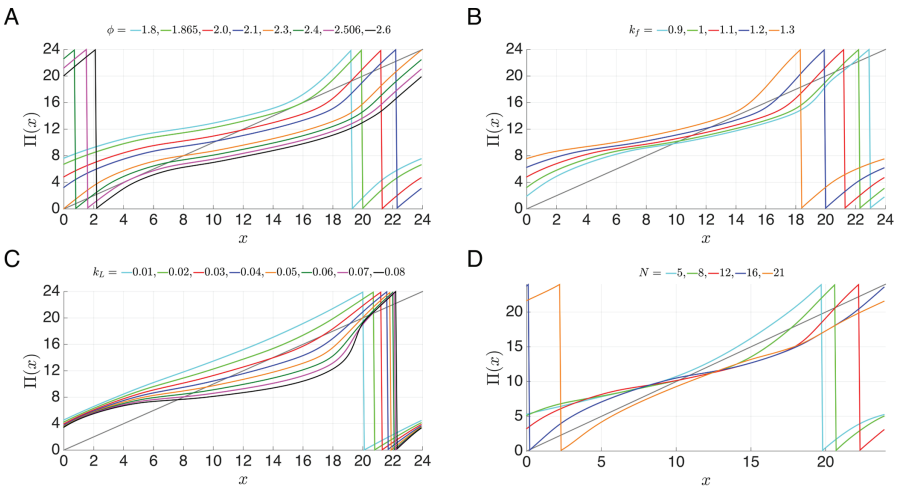

Figure 4. The entrainment map $\Pi(x)$ changes systematically as intrinsic (A, B) and extrinsic (C, D) model parameters are varied. (A, B) Increasing the intrinsic speed of oscillators by (A) increasing ϕ or (B) decreasing k_f moves the stable fixed point of the map to the left and leads to entrained oscillators that encounter light earlier in the subjective day. Loss of entrainment occurs when the curves do not intersect the diagonal. (C) Increasing k_L also moves the stable fixed point of the map to the left, corresponding to increased light intensity advancing the phase of entrainment. The increased concavity of $\Pi(x)$ as k_L increases suggests that brighter light decreases the amount of time required to reach stable entrainment. (D) Changes in light duration (N) have only a minor effect on the location of the stable fixed point of the map, suggesting that the photoperiod does not significantly affect the phase of entrainment for these parameter values. However, the fixed points do undergo saddle-node bifurcation if the light duration is too short or too long, corresponding to loss of entrainment in extreme photoperiods.

(x_1, x_2) as $(20.9-29.6)/(17.7-5) = -0.71 > -1$. Note from Figure 3B that along the decreasing portion, there exists a unique value $x_s \in (x_1, x_2)$ for which $\rho(x_s) = 24$. There is also another value x_u along the increasing portion of $\rho(x)$ for which $\rho(x_u) = 24$. Although it is obvious from our simulation results that x_s and x_u exist, analytically proving this fact is beyond the scope of this paper.

In Figure 3C, we show the graph of the map $\Pi(x)$. Note that x_s and x_u are fixed points of this map. Further, $\Pi'(x) = \rho'(x) + 1 > 0$ since $-1 < \rho'(x)$, implying that the graph of Π is increasing wherever it is continuous. It has a discontinuity whenever $\rho(x) + x$ passes through a multiple of 24. Finally, note that $|\Pi'(x_s)| < 1$, implying that x_s is a stable fixed point, whereas $\Pi'(x_u) > 1$, implying that x_u is an unstable fixed point. The stable fixed point x_s corresponds to a stable LD-entrained solution and is shown in Figure 3D. The stable fixed point occurs at $x_s = 10.2$, which means that when the LD-entrained solution starts on $\mathcal{P}$, it initially experiences 1.8 h of light. This is followed by 12 h of darkness, where the trajectory tracks the DD limit cycle. After this time, the trajectory is again subject to conditions of light, and it can be seen that the trajectory deviates from the DD limit cycle. Similarly, x_u corresponds to an unstable LD-entrained solution, which is also shown in Figure 3D. The value $x_u = 20.5$, so it initially experiences about 3.5 h of darkness when starting on $\mathcal{P}$ before then experiencing 12 h of light and then subsequent darkness. In some sense, for this set of parameters, its trajectory experiences light and darkness at opposite locations in phase space relative to the solution associated with x_s. Further consequences of the existence of x_s and x_u are explored below when we discuss the dynamics of entrainment.

Dependence of $\Pi(x)$ on Parameters

To study how the map depends on parameters, we start with the canonical set of parameters and systematically vary one at a time. We begin with the parameter ϕ, which determines the intrinsic period of the oscillator by controlling the rate of evolution of both the P and M variables. Larger ϕ implies a faster oscillator. If ϕ is too large, however, then the intrinsic period of the circadian clock is too small (much less than 24) and phase-locking with a 24-h forcing will not be possible. The same conclusion occurs when ϕ is too small and the circadian clock is too slow. Thus, there exists an interval (ϕ_{min}, ϕ_{max}) such that stable one-to-one entrainment occurs for ϕ lying in that interval. This is a standard result from the forced oscillator literature; see Glass (1991) for an example.

Supplementary Figure S1 shows that $\rho(x)$ shifts down when ϕ is increased. This makes sense as faster dynamics imply smaller transit times and so $\rho(x)$ should be smaller. In addition, $\rho(x)$ also shifts to the right, as explained in the Supplementary Material, Section R1. Figure 4A shows the map $\Pi(x)$ for several

different choices of ϕ. As ϕ increases, the curves shift down and to the right, the discontinuity moves to the right, and the stable fixed point x_s moves down and to the left. Biologically, this means that faster intrinsic oscillators encounter light earlier in the subjective day when entrained than do slower intrinsic oscillators. In other words, fast intrinsic oscillators have advanced phases of entrainment (morning larks) and slow intrinsic oscillators have delayed phases of entrainment (night owls) (Bordyugov et al., 2015). Note that as ϕ increases, the value of x_s increases from around 5 h at $\phi = 1.865$ to 15 h at $\phi = 2.506$. The value $\phi_{min} = 1.865$ corresponds to the saddle node bifurcation where the map lies above and tangent to the diagonal; $\phi_{max} = 2.506$ corresponds to a second saddle node bifurcation that occurs when the map lies below and tangent to the diagonal. The interval (ϕ_{min}, ϕ_{max}) is called the ϕ-range of entrainment. To understand the path through which entrainment is lost, note that as ϕ approaches ϕ_{min} from above or ϕ_{max} from below, the fixed points x_s and x_u merge in a saddle-node bifurcation. This merging corresponds to a saddle-node bifurcation of periodic orbits in phase space, as described in Supplementary Material, Section R1.

The parameter k_f is associated with positive feedback in the accumulation of protein due to inhibition of protein degradation (Novak and Tyson, 2008; Tyson et al., 1999). Increasing k_f moves the P-nullcline up in the phase space. However, this effect is much more pronounced on the left branch of the P-nullcline. As a result, the dynamics slow down near the left branch, more than they speed up away from it, resulting in a net slower speed. This causes $\Pi(x)$ to shift up and to the left and the stable fixed point x_s to move down and to the right (Fig. 4B). Thus, increasing the amount of positive feedback slows down the intrinsic oscillations (consistent with recent findings in other circadian models; Ananthasubramaniam and Herzel, 2014) and leads to entrained clocks encountering light later in the subjective day. When k_f increases to 1.27, the fixed points x_s and x_u merge at a saddle node bifurcation, indicating that too much positive feedback can lead to loss of entrainment. As k_f decreases, the fixed point along the middle branch of $\mathcal{N}_P$ eventually becomes stable, causing the disappearance of the LL oscillation at $k_f = 0.88$ and DD at $k_f = 0.70$. Note, however, that for $0 < k_f < 0.88$, even though we no longer have self-sustained LL and DD oscillations, it is still possible for the system to be driven by the forcing to exhibit 24-h rhythms. Mathematically, this occurs because in this range of k_f, the model reduces to driving a stable fixed point with the 24-h forcing. The ensuing limit cycle is relatively small in amplitude and lies in a neighborhood of the intersection of the $\mathcal{N}_P$ and $\mathcal{N}_M$ nullclines. From a circadian point of view, this is an example of "masking" rather than entrainment (Mrosovsky, 1999).

Understanding the effect of changes in k_L and N is somewhat more complicated than the changes due to ϕ and k_f. The reason is that changes in k_L dramatically affect the right branch of $\mathcal{N}_{P_L}$, while changes in N affect where in phase space the LD-entrained oscillator experiences conditions of light or dark. As a result, their respective effects on the speed of the LD-entrained oscillator are less uniform than with the intrinsic parameters.

Increases in light intensity are modeled by increasing k_L. For small values of k_L, entrainment is not possible, since the forced oscillator will still be too slow. Thus, there is a minimum strength of $k_L = 0.029$ needed to entrain. Over a range of values, increasing k_L speeds up the oscillations, since in general, the dynamics under lights are faster than during dark. Figure 4C shows the effect of changing k_L on the map Π. Because increases in k_L speed up the dynamics, the map shifts down and to the right (although there is small region near $x = 20$ where this is not true for the larger values of k_L) and the stable fixed point moves to the left. This corresponds to increased light intensity advancing the phase of entrainment. With our canonical parameter set, the intrinsic oscillator has a long DD period ($\tau > 24$) and a delayed phase of entrainment (i.e., a night owl). Thus, this result is consistent with the use of bright light therapy to treat patients with delayed sleep phase syndrome (Dodson and Zee, 2010). For this figure, we had to lower the Poincaré section to $M = 0.4$ to guarantee that for any initial condition of the map, the ensuing trajectory crossed $\mathcal{P}$ in the first cycle of its oscillation. Note that this results in $x_s = 9.76$ and $x_u = 20.0$ for the canonical case. Increased values of k_L cause the linear portion of the equation that determines $\mathcal{N}_{P_L}$ to dominate. In this case, $\mathcal{N}_{P_L}$ can become monotone increasing and nearly linear, which produces a stable fixed point at the intersection of $\mathcal{N}_M$ for $k_L = 0.089$. Thus, the LL limit cycle will fail to exist. Observe that for $k_L > 0.089$, although the LL oscillation fails to exist, the LD-entrained solution will continue to exist. For this case, during the light portion, the trajectory tracks the left branch of $\mathcal{N}_{P_L}$ toward the stable fixed point. This fixed point prohibits the trajectory from leaving $\mathcal{N}_{P_L}$ and, as a result, puts an upper bound on how fast the oscillator can evolve. When the lights turn off, the nullcline switches to $\mathcal{N}_{P_D}$, which is cubic shaped, and the trajectory circles the unstable intersection point of $\mathcal{N}_{P_D}$ and $\mathcal{N}_M$ before returning the left branch of $\mathcal{N}_{P_D}$. Thus, for arbitrarily large values of k_L, oscillations persist, such that increasing the intensity of light can speed up the oscillations only to a certain extent and never too fast to disrupt entrainment.

Figure 4D shows how the map $\Pi(x)$ depends on the photoperiod $N:24-N$ (LD). Increasing N means that the oscillator is exposed to more light. Generally, this does speed up the dynamics. This fact is reflected by the discontinuity x_d moving to the right as N increases, similar to how it moves for all the other parameter variations that speed up the dynamics. What differs with changes in N from other cases is that the map as a whole does not shift down and to the right. Entrainment continues to disappear through saddle node bifurcations if the LD forcing is too heavily skewed toward either the light or dark intervals. When N is large, the photoperiod contains too long an interval of light. The oscillator becomes too fast and loses the ability to entrain in the same way that entrainment is lost when ϕ increases. In particular, the left part of the map $\Pi(x)$ shifts down and to the right with increases in N just as it does with increases in ϕ. The right part of the map shifts up when N is decreased and the dark interval dominates. In that case, the oscillator eventually becomes too slow to entrain, similar to when ϕ is decreased. Further details explaining why the map behaves in this way are provided in the Supplementary Material, Section R1.

Dynamics of Entrainment

Having understood the situations that lead to the existence of the LD-entrained stable and unstable solutions, let us now turn to understanding some aspects of the transient dynamics of trajectories that start with initial conditions that lie off of these limit cycles. The most straightforward way to do this is to use the map Π to track the transient dynamics associated with an initial condition x_0. This will allow us to make comparisons to a direct simulation in which we start an oscillator on the Poincaré section $\mathcal{P}$, x_0 hours into an LD cycle.

For the map $x_{n+1}=\Pi(x_n)$, a cobweb diagram from any initial condition $x_0 \neq x_u$ shows that the trajectory converges to the stable fixed point x_s. We can readily determine 2 characteristics of entrainment: the time to entrainment and the direction of entrainment. In the Methods section, we defined a solution to be entrained if there exists m, such that for all $j \geq m$, $|x_s - x_j| < 0.5$. The integer m depends on x_0 and refers to the number of iterates needed for the condition to hold from any given initial condition x_0. We can calculate the time to entrainment in the following way. In the cobweb diagram, at each iterate, the trajectory hits either the upper or lower branch of Π. Let x_d denote the value of the discontinuity of the map. Depending on the location of the discontinuity x_d, the time $\rho(x)$ associated with that iterate will differ (see the Supplementary Material, Section R2, for details). The direction of entrainment refers to whether the cobwebbed iterate moves to the left or the right. When $x_{n+1} > x_n$, then the iterate moves to the right, and the phase of the oscillator with respect to the onset of the lights is larger. Thus, we call this a *phase delay*. Alternatively, we obtain a *phase advance* when the iterate moves to the left when $x_{n+1} < x_n$. Note, however, that transitions between branches follow a different rule. If $x_d > 12$, then a transition from the lower branch at one iterate to the upper branch at the next iterate is considered a phase delay, even though $x_{n+1} < x_n$. This is because this type of iterate is equivalent to more than 24 h passing before the return to $\mathcal{P}$. If $x_d < 12$, then the transition from upper branch to lower branch is considered a phase advance even though $x_{n+1} > x_n$, since this type of iterate implies 2 crossings within one 24-h cycle. Finally, observe that the unstable fixed point x_u demarcates which initial conditions lie on trajectories that entrain through phase advancing or phase delaying.

To study a specific example, we return to the map associated with the canonical set of parameters. Here $x_s = 10.2$, $x_u = 20.5$, and $x_d > 12$. Let us choose an initial condition $x_0 = 20.2$. This point lies to the left of x_u, so under the cobweb dynamics, it will move to the left and converge to x_s from above, thereby phase advancing (green trajectory of Fig. 5A). Comparing to direct simulations, we find that the entrainment time is 158.281 (6.6 days), which matches very well with the predictions of the map (157.247 h). As another example, choose $x_0 = 21.2$, which lies to the right of x_u. Now the iterates of the map move to the right, hit the lower branch of Π, and then are cobwebbed back to a smaller value of x, from where they continue moving right (magenta trajectory in Fig. 5A). In this case, the oscillator entrains through phase delaying. From the map, we find the entrainment time to be 180.775 h (7.5 days) and from direct simulations to be 180.767 h. In Figure 5B, we show the time traces for solutions with each of these 2 initial conditions. Note that the green trajectory phase advances, while the magenta trajectory phase delays, consistent with the predictions of the map. Explicit values calculated from iterates of the map and direct simulations are shown in Tables S1 and S2 in the Supplementary Material, Section R2.

The map allows us to easily calculate entrainment time for any initial condition, for a range of parameters. For example, to see how light intensity affects entrainment time, we varied the initial conditions between 0 to 24 for 3 different values of k_L; see Figure 6 (also see the Supplementary Material, Section R2, which shows how choosing a different Poincaré section affects entrainment time). The solid curve denotes the canonical case $k_L = 0.05$, while the dashed and dotted curves are for $k_L = 0.03$ and 0.08,

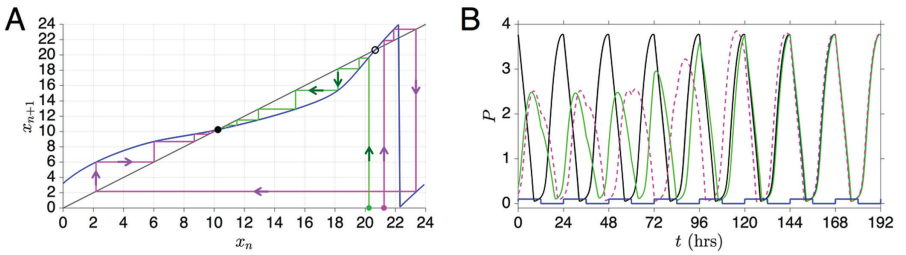

Figure 5. Entrainment maps systematically reveal entrainment dynamics such as whether entrainment will occur through phase advances or phase delays. (A) Cobweb diagram showing convergence to x_s starting from 2 different initial conditions $x_0 = 20.2$ (green trajectory) and $x_0 = 21.2$ (magenta trajectory). The former entrains by phase advancing, the latter by phase delaying. (B) The approach to the stable cycle shown in the t versus P plane. Green and magenta traces correspond to the same values as in part A.

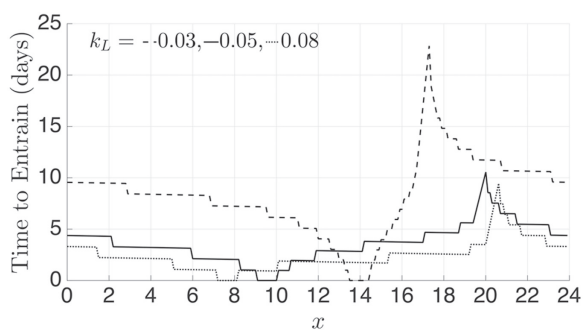

Figure 6. Time to entrain depends on light intensity and the proximity of initial phase to the stable and unstable fixed points. Larger values of k_L, on average, lead to faster entrainment. For each case, the minimum entrainment time of 0 occurs for initial conditions in a neighborhood of x_s and the maximum in a neighborhood of x_u ($x_s = 13.9, 9.5, 7.6$ and $x_u = 17.2, 20.0, 20.6$ for $k_L = 0.03, 0.05, 0.08$, respectively).

respectively. As expected, for each curve, initial conditions that start in a neighborhood of x_s (local minima of curve) take no time to entrain, while those in a neighborhood of x_u take the longest. Note that x_s and x_u change as a function of k_L, as can be seen from Figure 4C. Further note that stronger light ($k_L = 0.08$) leads, on average, to the shortest entrainment times, as can be observed by noting that the dotted curve lies on average below the others. This result can be predicted based on how the shape of $\Pi(x)$ changes with k_L. Observe from Figure 4C that as k_L increases, the map has a region where the slope becomes smaller (roughly between $x = 4$ and $x = 16$) and a region where the slope and concavity increase (roughly between $x = 16$ and $x = 20$). It is in the region $x = 10$ to 20 that entrainment time dramatically decreases for $k_L = 0.08$. The reason is that iterates of the map use this sharp change in slope to make bigger advances toward the fixed point. This suggests that the amount of time required for a circadian oscillator to reentrain following a phase shift in the light-dark cycle, for example, after rapid transmeridian travel, will depend on light intensity with brighter light resulting in less jetlag.

Relating $\Pi(x)$ to a PRC

The phase response curve of an oscillator measures the change in asymptotic phase experienced when a perturbation is given to an oscillator along different parts of its limit cycle. In the context of our problem, we shall construct the PRC using a light pulse of length N hours with $k_L = 0.05$. Specifically, start with a DD oscillator on the Poincaré section $\mathcal{P}$. Allow it to evolve for y hours along the DD limit cycle and then perturb it by introducing a light pulse of N hours. We define

$$Z_k(y) = k\tau - \tau_k(y), \tag{6}$$

where τ is the free running period of the DD oscillator and $\tau_k(y)$ is the time when the perturbed oscillator crosses $\mathcal{P}$ for the kth time. At each cycle, the quantity $Z_k(y)$ measures the deviation of the transit time of the perturbed oscillator from the DD oscillator. $Z_k(y)$ is often called the kth-order PRC. Here, phase 0 is chosen as a point on the DD oscillator and thus the perturbed phase is defined relative to the DD oscillator itself. In general, such PRCs are typically used when 2 conditions are met: The duration N of the light pulse is small, and the magnitude k_L is not too large. These conditions imply that the effect of the light pulse is felt within the current or subsequent cycle to when it is applied and that the oscillator returns quickly to its intrinsic limit cycle thereafter, albeit with a potentially different phase. Both in theory and, as we will show, in practice, these conditions limit the applicability of using PRCs to determine phase-locking.

The map $\Pi(x)$ can be directly compared to $Z_k(y)$ provided that both functions have the same domain. First, note that the domain of Z_k is the interval $[0, \tau]$, while the domain for Π is $[0, 24]$. Thus, the 2 functions can be compared only when $\tau = 24$ or by truncating the domain of Z_k (if $\tau > 24$) or Π (if $\tau < 24$). To consider a case of $\tau = 24$, we set $\varepsilon = 0.01$ and $\phi = 8.07$. In turn, this implies that $\tau_1(y) = \rho(x)$ and $x + y = 24$, as shown in Figure S3 of the Supplementary

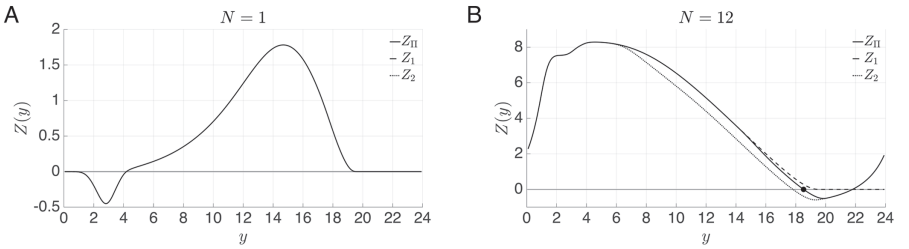

Figure 7. The PRC fails to accurately predict the phase of entrainment for long light pulses, whereas the entrainment map is accurate for light pulses of any length. (A) For a short light pulse ($N = 1$), Z_1, Z_2, and Z_Π all agree with one another. (B) For a longer light pulse ($N = 12$), only Z_Π correctly predicts the value of the root computed by direct simulation (solid dot at $y = 18.522$).

Material, Section R3. Substitute into Equation (6) for $k = 1$ to obtain

$$Z_\Pi(y) = \tau - \rho(24 - y). \tag{7}$$

The subscript on the PRC in this case indicates that this function is obtained from our map Π rather than directly through simulation. Additionally, it is convenient to leave $Z_\Pi(y)$ expressed in terms of $\rho(24 - y)$ rather than in terms of Π so that we can avoid the mod operation.

In Figure 7A, we show the results of directly computing the PRCs $Z_1(y)$ and $Z_2(y)$ for $N = 1$ and $\tau = 24$ with the map-based PRC $Z_\Pi(y)$. Note that because the effect of a single light pulse wears off relatively quickly, $Z_{k+1}(y) = Z_k(y)$ for $k \geq 2$. A stable phase-locked solution will occur where the PRC has a root with negative slope. All 3 PRCs quantitatively agree with one another, although it is difficult to discern that the PRC is non-zero for small and large values of y. In Figure 7B, we show the results for a case where the duration of the light pulse is not small, specifically $N = 12$. Note here that $Z_1(y)$, $Z_2(y)$, and $Z_\Pi(y)$ differ quantitatively for larger values of y. In particular, all 3 have different stable roots. By comparison to direct simulations, the roots predicted by $Z_1(y)$ and $Z_2(y)$ are incorrect, whereas the root predicted by the map-based $Z_\Pi(y)$ is correct.

The preceding example of $N = 12$ allows us to illustrate the primary difference between the entrainment map Π and the PRC, as well as the limitations of the latter. In Figure 8A, we show schematic diagrams of the case where y is chosen as the root of $Z_\Pi(y)$ ($y = 18.522$), which depicts where in time the oscillator is subjected to light. Figures 8B, 8C, and 8D show trajectories in the phase plane. In Figure 8A, the first solid line of each schematic denotes $t = 0$ and represents the trajectory starting on the Poincaré section $\mathcal{P}$. For the map $\Pi(x)$, $x = 24 - y$ is small (since y is large), and thus the trajectory starts out with the lights on. In the phase plane, the trajectory will follow the LL cycle for $12 - x$ hours, before then following the DD dynamics for 12 h. After that time, the trajectory will again be subjected to light during the remaining time x it takes to return back to $\mathcal{P}$. Thus, when constructing the entrainment map Π, the light pulse is allowed to be split up over different portions of the cell's trajectory, as shown in Figure 8B. In contrast, when constructing the PRCs $Z_1(y)$ and $Z_2(y)$, the light pulse is never split up. In the phase space, the trajectory now traverses along DD for y hours before the lights turn on. Thus, in comparison to the Π-based trajectory, it is in a very different location in phase space when the LL dynamics come into play. The first crossing of P yields $Z_1(y)$. As can be seen from Figure 8C, the oscillator has received only a small portion of the light pulse to this point, but it receives the light in a region of phase space that speeds up its oscillation. The second solid orange line in Figure 8A shows where the oscillator is relative to the light cycle at the moment it again crosses $\mathcal{P}$. The light gray lines show 24-h intervals and represent where the oscillator would have been in the absence of light input. Thus, $Z_1(y) > 0$. After this point, the trajectory receives the remaining portion of light shown in Figure 8D but is actually in a region of phase space where the added light slows it down (lower schematic of Fig. 8A). In fact, it is slowed down so much that at the second crossing of $\mathcal{P}$, $Z_2(y) < 0$.

When the intrinsic period of the DD oscillator is different than 24 h, then we must restrict the domain of $Z_k(y)$ or $\Pi(x)$ to be able to directly compare them. Alternatively, we can simply compare the predictions regarding the phase of locking made by the map $\Pi(x)$ versus those made by either $Z_1(y)$ or $Z_2(y)$. We did so over a set of ϕ values (from $\phi = 5.5$ to 8.25, with $\varepsilon = 0.01$) that span a range of intrinsic periods τ from 23.5 to 35.2. In all cases, when compared to direct simulations, the predictions made by the map Π were more accurate than those made via the PRCs; for details, see Table S3 in the Supplementary Material, Section R3. We also checked the accuracy of the predicted phase of entrainment for an alternative PRC construction protocol that was based on detecting

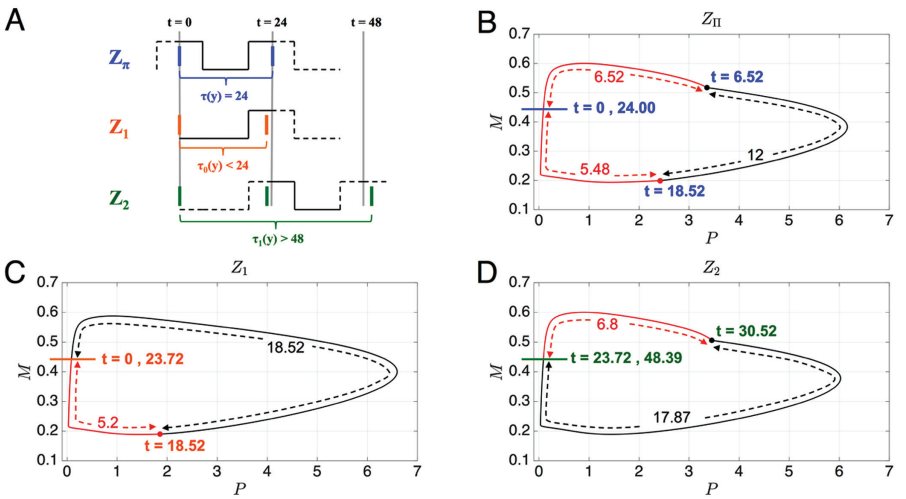

Figure 8. Comparison of how the light pulse affects the calculation made by the various PRCs. (A) Schematic showing where in time the oscillator crosses $\mathcal{P}$ (solid blue, orange, and green) and where the reference oscillator does for Z_1 and Z_2 (solid gray). The portion of the light pulse that is used in the calculation is shown in solid in each case. (B-D) Each panel shows where in phase space the light pulse affects the oscillator. (B) Effect of light pulse is split up in time, $t = 0$ to $t = 6.52$, and then again from $t = 18.52$ to $t = 24$. (C) The light pulse is only felt at the end of the oscillation from $t = 18.52$ to $t = 23.72$. (D) The light pulse is only felt during $t = 23.72$ to 30.52.

peaks of the P variable rather than crossings of a Poincaré section. Specifically, we perturbed the canonical DD oscillator ($\phi = 2.1, \varepsilon = 0.05$) with light pulses ($k_L = 0.05$) and then measured the phase shift of the peak time in the sixth cycle after the perturbation. The PRC predicted the entrained phase correctly (within 2-min accuracy) for $N = 12$ but was off by more than 30 min for $N = 16$. In contrast, the entrainment map predicted the entrained phase correctly (within 1 second accuracy) in both cases.

Higher Dimensional Models

We now show that the entrainment map can be defined in higher dimensional settings by constructing maps for the Gonze and Kim-Forger models. In each of these cases, the Poincaré section is chosen at a fixed value of a variable that does not receive the light-dark forcing $f(t)$ as described in the Methods section. Note that in addition to being of different dimensionality, these models also differ in the manner in which light enters the equations. In the fly model (NT), light increases the rate of protein degradation, whereas in the mammalian models (Gonze and Kim-Forger), light increases the rate of mRNA transcription. These distinct effects of light lead to contrasting relationships between DD and LL dynamics across the models. Specifically, the LL limit cycle has a shorter period than the corresponding DD limit cycle in the NT model but a longer period than the corresponding DD limit cycle in the Gonze and Kim-Forger models. Despite these differences in the behavior of these models under constant dark and constant light conditions, we find that the entrainment maps for these models share some common features and are able to accurately capture the effects of light-dark forcing in all 3 cases.

Figures 9A and 9B show the entrainment maps for 3 different values of the intrinsic periods of the respective models. Although it is difficult to see, note that as the intrinsic oscillator speeds up (increasing ϕ), the maps move the same way as they did in the NT model. Namely, the entrained phase shifts to an earlier part of the light-dark cycle. The maps for both models also share with the NT maps the property of having 1 point of discontinuity. This commonality across the 3 models, together with those discussed below, suggests that the entrainment map provides a robust method for finding universal properties of circadian oscillators.

In Figures 9C and 9D, we show how the maps behave in response to increases in light intensity (ν_L in the Gonze model and tr_L in the Kim-Forger model). In both models, as light is increased, the phase of entrainment does not change much. Instead, at various places, the concavity of the map increases. As these properties were also found in the NT model (Fig. 6), we would predict that stronger light leads to faster entrainment in both of these models just as it did in the NT model.

In Figures 9E and 9F, the PRCs $Z_\Pi(y)$, $Z_1(y)$, and $Z_2(y)$ are shown for a 12:12 photoperiod. What is interesting about these graphs is how poorly the

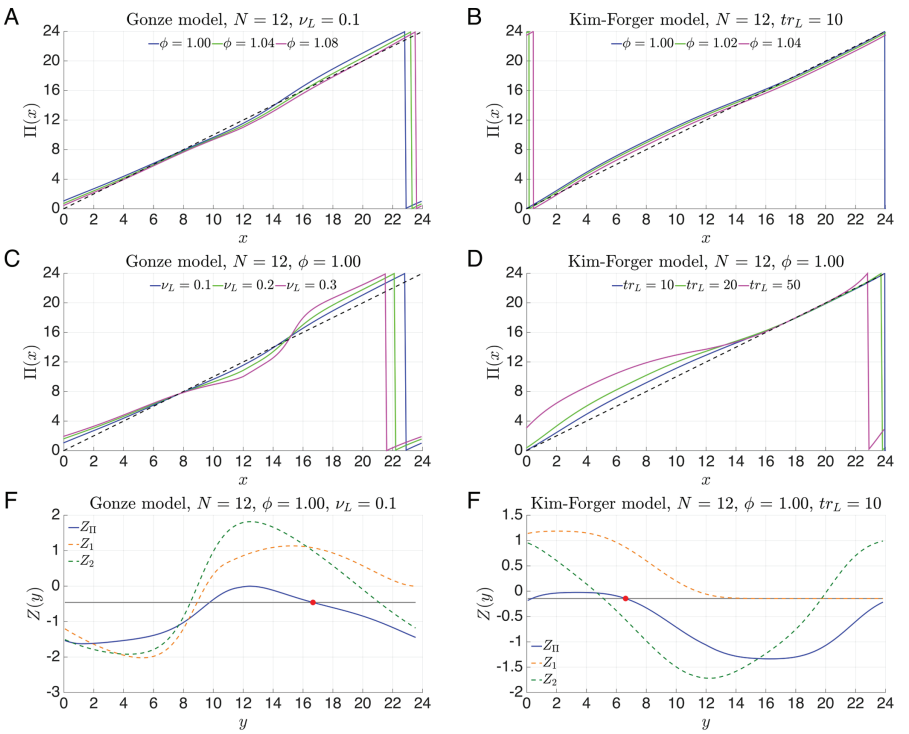

Figure 9. Entrainment maps and PRCs for the Gonze model (left) and Kim-Forger model (right). (A and B) Variations in the maps due to changes in the intrinsic period of the oscillators. As with the NT model Figure 4A, the map shifts down and to the right for faster intrinsic oscillators. (C and D) Stronger light affects entrainment. There is not much difference in the phase of entrainment but a pronounced difference in the concavity of the map, which will lead to faster entrainment. (E and F) Comparisons of the PRC generated from our map, $Z_\Pi(y)$, versus those generated from perturbations of the DD limit cycle. The red dot is the entrained phase calculated via direct simulation.

conventional PRCs Z_1 and Z_2 perform in predicting the entrained phase (red dots). Z_1 fails to produce an entrained phase for the Gonze model while producing a set of nonunique solutions for the Kim-Forger model. Z_2 is quantitatively incorrect for both models. The reason why the conventional PRC fails is because it is calculated using a perturbation of the DD limit cycle. In contrast, the entrainment map based PRC, Z_Π, perturbs off of the LD-entrained solution and produces an accurate prediction. For the Gonze model, it is possible to see that the DD and LD-entrained solutions lie in very different regions of phase space (see Suppl. Fig. S5). So the fact that the PRC and map-based predictions are different is not surprising. For the Kim-Forger model, it is nearly impossible to tell where in phase space the DD and LD-entrained solutions lie. But we would infer that they are not near one another.

DISCUSSION

Circadian rhythms enable organisms to appropriately align physiological and behavioral processes with the 24-h environmental cycles conferred by the earth's daily rotation. Rhythms persist when the organism is isolated from external time cues; however, in constant conditions the period of circadian oscillators is typically not exactly 24 h. For example, the average human circadian rhythm is 24.2 h while that of mice is 23.5 h (Ripperger et al., 2011). These oscillators are subject to periodic external forcing such as the light-dark cycle that adjusts the phase of the rhythm and entrains them to a period of 24 h. The entrained rhythm must have the proper phasing with respect to external events in order for the circadian system to confer a selective advantage to the organism (Ben-Shlomo and Kyriacou, 2002). Two important questions arise: Under what conditions do circadian oscillators phase-lock to external forcing, and when they do what determines the phase of entrainment?

In this paper, we have developed a new method to determine the phase-locking properties of a circadian oscillator relative to a 24-h light-dark cycle. We derived an entrainment map $\Pi(x)$ for a 2-dimensional NT model of the *Drosophila* molecular circadian clock and then showed that the map can be similarly derived for the 3-dimensional Gonze and the 180-dimensional Kim-Forger models of the mammalian molecular circadian clock. In particular, if the

oscillator lies on a Poincaré section $\mathcal{P}$ and x is the time from the onset of the most recent light-dark cycle, $\Pi(x)$ is measured when the oscillator first returns to $\mathcal{P}$ and predicts the time from the beginning of the most recent light-dark cycle. A fixed point of the map corresponds to a phase-locked LD-entrained solution. In all models, for canonical sets of parameters, we showed that the map typically has 2 fixed points, x_s, which is stable, and x_u, which is unstable. Further, since $x = 0$ corresponds to where the lights turn on (nominally 0700 h), knowing the value of x_s allows us to determine where along the trajectory in phase space the lights turn on and off. For example, in the NT model with the set of parameters that corresponds to an intrinsic period $\tau = 27.6$ (canonical parameter set with $\phi = 2.2$), the LD-entrained solution has the lights turn on 14 h before M reaches its maximum value. This is consistent with biological findings that the highest mRNA levels for *Per*, an important gene in the *Drosophila* circadian clock, are found 2 h after lights off in a 12-h:12-h light-dark cycle (Young, 1989).

Using the entrainment map allowed us to understand and predict the effects of parameter changes in the model. Indeed, parameters that have similar effects influence the entrainment map in the same way across all 3 models. For example, increasing ϕ decreases the intrinsic period of the oscillators. In all cases, the entrainment map $\Pi(x)$ shifts down and to the right, moving the stable fixed point x_s to smaller values. The analysis also revealed several interesting roles for the unstable fixed point x_u. First, x_u separates the set of initial conditions x_0 that entrain via phase advance or phase delay. Second, initial conditions that are in a neighborhood of x_u took the longest to entrain, largely independent of the direction of entrainment. Third, loss of entrainment could occur due to changes in parameters through a stereotypical saddle-node bifurcation when x_s and x_u merge. Some changes in parameters, however, never lead to a loss of entrainment: in particular, increases in light intensity (k_L in NT, ν_L in Gonze, and tr_L in Kim-Forger). Fourth, the existence of x_u implies the existence of an unstable entrained periodic solution. As shown in Figure 3D, this unstable limit cycle is smaller in amplitude than its stable counterpart. It is also shifted by a distance of roughly $|x_s - x_u|$ in terms of when it experiences light relative to the stable limit cycle. For the canonical set of parameters, this implies that when the unstable limit cycle is experiencing light, the stable limit cycle is experiencing dark, and vice versa. Thus, the solutions are effectively 180° out of phase. As ϕ changes and the system nears a saddle-node bifurcation, the difference in phases between the stable and unstable solutions shrinks (eventually going to 0) and entrainment occurs mostly through phase advance if $x_s > x_u$ or phase delay if $x_s < x_u$.

The basic idea behind constructing an entrainment map for any particular model is quite general. Namely, in the phase space of the model, choose a Poincaré section along a point of the LD-entrained solution. Then compute the map $\Pi(x)$ by taking initial conditions that lie at the intersection of the map and the LD-entrained solution and measure the return time to the Poincaré section. $\Pi(x)$ is then the amount of time that has passed since the onset of lights in the most recent light-dark cycle. As such, the entrainment map will always be 1-dimensional. What will vary is the dimensionality of the Poincaré section $\mathcal{P}$. As our simulations have shown, even when the Poincaré section is high dimensional, as in the Kim-Forger model, the entrainment map very accurately predicts the stable phase of entrainment. In these high-dimensional cases, the map has the added advantage that effects of changes in parameters are more easily predicted because these changes are stereotypical across models.

Comparison to Prior Work

There are 2 major paradigms for entrainment in the circadian field: discrete (or nonparametric) entrainment and continuous (or parametric) entrainment (Roenneberg et al., 2010a). The former is based on the idea of a free-running oscillator, DD for example, experiencing discrete phase shifts in response to perturbative inputs along its limit cycle and in particular light-dark transitions. This approach has led to methods based on the PRC and does not explicitly take into account the periodic nature of the forcing signal. The second paradigm assumes that entrainment occurs through continuous adjustments to the speed of the oscillator and involves a velocity response curve (VRC) (Beersma et al., 1999; Rand et al., 2004; Taylor et al., 2010, 2014). The VRC characterizes regions in the circadian phase space where the speed of the oscillator increases or decreases as a function of a change of parameter—for example, light intensity. It can be thought of as the variational derivative of the phase with respect to a parameter of interest. This approach is categorized as being continuous, rather than discrete, because it assumes that light affects the oscillator throughout the circadian cycle and not just at light-dark transitions. Both PRC- and VRC-based methods are fundamentally based on using the isochron structure of the underlying DD oscillator to determine the change in phase. The phase of these oscillators is defined relative to a reference point on the DD oscillator itself.

Our approach to studying entrainment is different than these methods in that we view the periodic 24-h light-dark forcing as being the underlying rhythm that sets the reference point for determining phase. Namely we assign the time at which lights turn on as the reference $x = 0$ and do not separately define a phase for the DD or LL oscillators. We determine how a circadian oscillator with a prescribed initial condition relative to lights-on adjusts its dynamics over a periodic 24-h light-dark cycle. By considering the 24-h range of possible initial conditions, we obtain the entrainment map $\Pi(x)$. Depending on the initial condition, $\Pi(x)$ is calculated by splitting up either the light or dark pulse over the course of 1 or more 24-h cycles. For example, with 12:12 LD forcing, since $x = 0$ corresponds to lights-on, the initial condition $x_0 = 4$ leads to a computation that starts with the oscillator at $\mathcal{P}$ and imposes 8 h of light, followed by 12 h of dark and then 12 h of light and so on. The value $\Pi(4)$ is determined when the trajectory first returns to $\mathcal{P}$ independent of whether this time took less than, more than, or the same as 24 h. If, for example, $x_0 = 19$, then initially 5 h of dark would be imposed followed by 12 h of light, then 12 h of dark, and so on. In the former case, the light pulse would be split up; in the latter, the dark pulse would be split up. In contrast, PRC- and VRC-based methods only use a single light pulse, and often after imposing too long a dark duration (because they perturb off of DD conditions), which can lead to only a portion of the light pulse being taken into account by the time the oscillator returns to its reference phase.

The entrainment map is similar in spirit to the circadian integrated response characteristic (CIRC), proposed by Roenneberg et al. (2010b), in that both approaches attempt to take into account the periodic nature of the light-dark forcing. Common to all approaches is the need for a well-defined oscillatory solution that can be described as a limit cycle in an appropriate phase space. In most cases, this is the DD limit cycle. The entrainment map, in addition, uses the structure of the LL limit cycle to help define its properties. This is closely related to the suggestion by Peterson (1980), who noted that an LD-entrained solution at some moments in its cycle tries to approach the stable DD cycle and at other moments approaches the LL cycle. Our analysis involving $\Pi(x)$ does not explicitly incorporate a VRC. However, it does use the fact that changes in parameters differentially affect the speed with which a trajectory evolves in different regions of phase space. For example, we showed how changes to intrinsic parameters ϕ and k_f of the NT model had a more uniform effect on speed compared with those associated with the intensity k_L and duration N of the light pulse.

These points of difference and commonality aside, the entrainment map is simply a tool to make predictions about the phase-locking properties of a circadian oscillator. As a result, the findings obtained through its use should qualitatively match prior findings that use other methods that themselves match to empirical data. In Bordyugov et al. (2015), the authors derive conditions on entrainment and its dependence on parameters in an abstract setting of the Kuramoto phase oscillator model (Kuramoto, 1984). They then test the predictions made by the phase model on a modified Goodwin model of gene regulation with solely negative feedback (i.e., the Gonze model; Gonze et al., 2005) and on a 19-dimensional molecular clock model (Relogio et al., 2011). They consider a 2-dimensional parameter space consisting of the mismatch between the free-running period of the intrinsic oscillator and the period of the forcing and the relative strength of zeitgeber input to the oscillator amplitude. Their primary finding is that the one-to-one phase-locked solutions form a wedge-like structure (Arnold tongue) in this space and that the range of stable phases that exist within this wedge can span as much as 12 h. In particular, for weak zeitgebers, the 12-h span is achieved over a relatively small span of mismatches in the periods. As relative zeitgeber strength is increased, a larger range of period mismatch is needed to achieve the 12-h span of stable phases. This result is based on some earlier work of Granada and Herzel (Granada et al., 2013) that established the so-called 180° rule, which is another way to say that the range of stable phases spans 12 out of 24 h. Our results are very similar. For example, in Figure 4A, different values of ϕ correspond to different free-running periods of the DD oscillator. Since we held the forcing period constant at 24, changes in ϕ correspond to changing the period mismatch, or equivalently to considering a horizontal slice of the Arnold tongue in Figure 1A of Bordyugov et al. (2015). We see from Figure 4A that the range of stable phases spans roughly an 11-h range ($x_s \approx 15.8$ when $\phi = 1.865$ to $x_s \approx 4.8$ when $\phi = 2.506$). Using the entrainment map, we could also create a 2-parameter Arnold tongue representation, say for ϕ and k_L. To do so, we would combine results from Figures 4A and 4C. The Arnold tongue would also be wedged-shaped in the $\phi - k_L$ space. For fixed k_L, a horizontal slice is obtained by varying ϕ between ϕ_{min} and ϕ_{max}, as discussed above. For fixed ϕ, a vertical slice of the Arnold tongue could be obtained from Figure 4C, which shows that entrainment is lost when k_L decreases (creating a lower edge of the Arnold tongue) but persists as k_L increases.

Granada and Herzel (2009) studied how the time to entrainment is affected by various parameters. One of their main findings, derived for an abstract

Poincaré oscillator and then applied to a Goodwin model, is that larger relative zeitgeber strengths leads to faster average entrainment. Their study was specifically designed to minimize the impact of different initial conditions of the oscillators. In our work, we can use the entrainment map to quickly calculate the entrainment time for any initial condition for any fixed set of parameters. Figure 6 shows results for different values of k_L, which is our equivalent to zeitgeber strength. As can be seen from that figure, increases in k_L do result in an average faster entrainment. This can be concluded by visual inspection that the area under the curves decreases as k_L increases. Our work additionally suggests that initial conditions that lie in a neighborhood of the unstable fixed point can take arbitrarily long times to entrain.

From a more mathematical point view, since $\Pi(x)$ is a circle map, our findings are consistent with the vast literature on forced oscillator models. In the general theory, when a specific parameter is varied, the forced system transitions through a series of different phase-locked (called $m:n$ solutions) and quasi-periodic (often called dense orbits) states. The $m:n$ solutions are actual periodic solutions of the map. These types of solutions occur when the mismatch between the intrinsic oscillator period and the forcing period leads to a rational rotation number, roughly defined as the ratio of oscillator period to forcing period. Dense orbits arise when the rotation number is irrational. These results are a consequence of Denjoy's theorem on circle maps and subsequent work of Arnold and many others (Arnold, 1965; Glass, 1991; Keener and Glass, 1984). Prior work shows that under certain assumptions, the rotation number varies continuously with a parameter of interest and that there exist parameter intervals over which different $m:n$ solutions can be found. In our case, we focused on one-to-one phase locking, showing that there is an interval (ϕ_{min}, ϕ_{max}) for stable entrainment. We did not exhaustively explore the existence of dense orbits or other solutions with rational rotation numbers, but we expect those to exist. Circle maps are also widely used in other contexts such as cardiac dynamics and, more generally, any process that involves clocking (Winfree, 2001). In such cases, a phase transition curve (PTC) is used to build a map to predict the effect of periodic forcing. The PTC measures the normalized phase of resetting as a function of the normalized stimulus phase. By *normalized* we mean that phase values lie between 0 and 1. The associated map at each cycle then measures the new phase as a function of the old. The PTC, therefore, is constructed using the PRC. Thus, PTCs face the same limitations in their use that PRCs do and can make predictions that are not borne out by a direct simulation or experiment; see Glass et al. (2002).

Future Directions

In this paper we have focused on light-dark forcing since it is the dominant zeitgeber for circadian clocks. However, the entrainment map can readily be extended to nonphotic entraining signals, such as temperature cycles, and perhaps give insight into how the circadian system integrates information from multiple environmental signals occurring simultaneously. The ease with which time to reentrainment can be calculated and visualized for different initial conditions by cobwebbing makes the map a useful tool for investigating jetlag scenarios. The map may also prove to be an effective tool for studying entrainment and synchronization in networks of coupled oscillators.

Entrainment maps of detailed molecular clock models such as Kim-Forger can be used to generate hypotheses about how specific mutations or other manipulations of clock components affect entrainment and to make predictions regarding entrainment mechanisms that can then be tested experimentally. One interesting question to explore using entrainment maps is the effect that different proposed mechanisms of transcriptional regulation (such as protein sequestration and Hill-type repression) have on entrainment properties (Kim et al., 2014; Kim, 2016).

Beyond circadian oscillator models, we believe that entrainment maps can also be successfully constructed based on data from real organisms or experimental preparations. To illustrate our suggested protocol, we consider the cyanobacterial circadian clock, for which the phosphorylation status of the protein KaiC is a convenient phase marker both in vivo and in vitro (Kim et al., 2015). To construct phase response curves for in vivo cultures, experimentalists maintain the cultures in constant light and then expose them to 4-h dark pulses at different phases and measure the resulting phase shift (Kim et al., 2012). To construct an entrainment map, we would instead maintain the cultures under a 12:12 LD cycle. The minimum of the KaiC phosphorylation waveform will play a role analogous to the Poincaré section $\mathcal{P}$. Once the culture is entrained, there will be a stable phase relationship between the onset of lights and the minimum of the KaiC phosphorylation rhythm. This gives us one data point for the map, namely the stable fixed point $x = \Pi(x)$. To obtain other data points, we will measure how the entrained oscillator responds to phase shifts in the LD cycle. Specifically, in one cycle we will extend the light or dark duration by a certain number of hours and then record the time of 2 subsequent minima of the KaiC phosphorylation waveform. This will give us an ordered pair $(x, \Pi(x))$. In fact, each KaiC phosphorylation minimum observed until the culture reentrains

will give us one additional data point for the map. Once the culture has reentrained, we can repeat the experiment with a different phase shift of the LD cycle to sample other areas of the map. Alternatively, the experiment can be done in parallel rather than serially by dividing the cyanobacterial culture into a population of subcultures and applying different LD phase shifts to each subculture.

ACKNOWLEDGMENTS

We thank Horacio Rotstein for helpful discussions regarding forced oscillators and Yong-Ick Kim for discussions about the cyanobacterial circadian clock. This work was supported in part by the National Science Foundation DMS-1412877 (C.D.), DMS-1555237 (C.D.) and DMS-1122291 (A.B.).

CONFLICT OF INTEREST STATEMENT

The author(s) have no potential conflicts of interest with respect to the research, authorship, and/or publication of this article.

NOTE

Supplementary material is available on the journal's website at http://jbr.sagepub.com/supplemental.

REFERENCES

Ananthasubramaniam B and Herzel H (2014) Positive feedback promotes oscillations in negative feedback loops. PLoS Comput Biol 10:e1003565.

Ananthasubramaniam B, Herzog E, and Herzel H (2014) Timing of neuropeptide coupling determines synchrony and entrainment in the mammalian circadian clock. PLoS Comput Biol 10:e1003565.

Arnold V (1965) Small denominators, I: mappings of the circumference onto itself. Am Math Soc Transl 46:213-284.

Bagheri N, Taylor S, Meeker M, Petzold L, and Doyle F (2008) Synchrony and entrainment properties of robust circadian oscillators. J R Soc Interface 5:S17-S28.

Beersma D, Daan S, and Hut R (1999) Accuracy of circadian entrainment under fluctuating light conditions: contributions of phase and period responses. J Biol Rhythms 14:320-329.

Ben-Shlomo R and Kyriacou B (2002) Circadian rhythm entrainment in flies and mammals. Cell Biochem Biophys 37:141-156.

Bordyugov G, Granada A, and Herzel H (2013a) How coupling determines the entrainment of circadian clocks. Eur Phys J B 82:227-234.

Bordyugov G, Westermark P, Korencic A, Bernard S, and Herzel H (2013b) Mathematical modeling in chronobiology. Handbook Exp Pharmacol 217:335-357.

Bordyugov G, Abraham U, Granada A, Rose P, Imkeller K, Kramer A, and Herzel H (2015) Tuning the phase of circadian entrainment. J R Soc Interface 12:20150282.

Dodson E and Zee P (2010) Therapeutics for circadian rhythm sleep disorders. Sleep Med Clin 5:701-715.

Forger D and Peskin C (2003) A detailed predictive model of the mammalian circadian clock. Proc Natl Acad Sci U S A 100:14806-14811.

Forger D, Gonze D, Virshup D, and Welsh D (2007) Beyond intuitive modeling: combining biophysical models with innovative experiments to move the circadian clock field forward. J Biol Rhythms 22:200-210.

Glass L (1991) Cardiac rhythms and circle-maps—a classical problem. Chaos 1:13-19.

Glass L, Nagai Y, Hall K, Talajic M, and Nattel S (2002) Predicting the entrainment of reentrant cardiac waves using phase resetting curves. Phys Rev E 65:021908.

Golombek D and Rosenstein R (2010) Physiology of circadian entrainment. Physiol Rev 90:1063-1102.

Gonze D (2011) Modeling circadian clocks: from equations to oscillations. Cent Eur J Biol 6:699-711.

Gonze D, Bernard S, Waltermann C, Kramer A, and Herzel H (2005) Spontaneous synchronization of coupled circadian oscillators. Biophys J 89:120-129.

Goodwin B (1965) Oscillatory behavior in enzymatic control processes. Adv Enzyme Regul 3:425-428.

Granada A and Herzel H (2009) How to achieve fast entrainment? The timescale to synchronization. PLoS One 4:e7057.

Granada A, Bordyugov G, Kramer A, and Herzel H (2013) Human chronotypes from a theoretical perspective. PLoS One 8:e59464.

Gu C, Liu Z, Schwartz W, and Indic P (2012) Photic desynchronization of two subgroups of circadian oscillators in a network model of the suprachiasmatic nucleus with dispersed coupling strengths. PLoS One 7:e36900.

Gu C, Xu J, Liu Z, and Rohling J (2013) Entrainment range of nonidentical circadian oscillators by a light-dark cycle. Phys Rev E Stat Nonlin Soft Matter Phys 88:022702.

Hirsch M, Smale S, and Devaney R (2013) *Differential Equations, Dynamical Systems, and an Introduction to Chaos*. Oxford, UK: Elsevier.

Indic P, Gurdziel K, Kronauer R, and Klerman E (2006) Development of a two-dimension manifold to represent high dimension mathematical models of the intracellular mammalian circadian clock. J Biol Rhythms 21:222-232.

Johnson C (1999) Forty years of PRCs—what have we learned? Chronobiol Int 16:711-743.

Johnson C, Elliot J, and Foster R (2003) Entrainment of circadian programs. Chronobiol Int 20:741-774.

Keener J and Glass L (1984) Global bifurcation of a periodically forced nonlinear oscillator. J Math Biol 21: 175-190.

Kim J (2016) Protein sequestration versus Hill-type repression in circadian clock models. IET Syst Biol 10: 125-135.

Kim J and Forger D (2012) A mechanism for robust circadian timekeeping via stoichiometric balance. Mol Syst Biol 8:630.

Kim J, Kilpatrick Z, Bennett M, and Josic K (2014) Molecular mechanisms that regulation the coupled period of the mammalian circadian clock. Biophys J 106:2071-2081.

Kim Y, Vinyard D, Ananyev G, Dismukes G, and Golden S (2012) Oxidized quinones signal onset of darkness directly to the cyanobacterial circadian oscillator. Proc Natl Acad Sci U S A 109:17765-17769.

Kim Y, Boyd J, Espinosa J, and Golden S (2015) Detecting KaiC phosphorylation rhythms of the cyanobacterial circadian oscillator in vitro and in vivo. Methods Enzymol 551:153-173.

Kuramoto Y (1984) *Chemical Oscillations, Waves, and Turbulence*. Heidelberg, Germany: Springer.

Leise T and Siegelmann H (2006) Dynamics of a multistage circadian system. J Biol Rhythms 21:314-323.

Leloup J and Goldbeter A (2013) Critical phase shifts slow down circadian clock recovery: implications for jet lag. J Theor Biol 333:47-57.

Mrosovsky N (1999) Masking: history, definitions, and measurement. Chronobiol Int 16:415-429.

Novak B and Tyson J (2008) Design principles of biochemical oscillators. Nat Rev Mol Cell Biol 9:981-991.

Peterson E (1980) A limit cycle interpretation of a mosquito circadian oscillator. J Theor Biol 84:281-310.

Pittendrigh C (1981) Circadian systems: entrainment. In *Handbook of Behavioral Neurobiology* (Vol 4), Aschoff J, ed, pp 95-124. New York: Plenum Press.

Ramkisoensing A, Gu C, van Engeldorp Gastelaars H, Michel S, Deboer T, Rohling J, and Meijer J (2014) Enhanced phase resetting in the synchronized suprachiasmatic nucleus network. J Biol Rhythms 29:4-15.

Rand D, Shulgin B, Salazar D, and Millar A (2004) Design principles underlying circadian clocks. J R Soc Interface 1:119-130.

Relogio A, Westermark P, Wallach T, Schellenberg K, Kramer A, and Herzel H (2011) Tuning the mammalian circadian clock: robust synergy of two loops. PLoS Comput Biol 7:e1002309.

Ripperger J, Judd C, and Albrecht U (2011) The daily rhythm of mice. FEBS Lett 585:1384-1392.

Roenneberg T, Daan S, and Merrow M (2003) The art of entrainment. J Biol Rhythms 18:183-194.

Roenneberg T, Chua E, Bernardo R, and Mendoza E (2008) Modelling biological rhythms. Curr Biol 18:R826-R835.

Roenneberg T, Hut R, Daan S, and Merrow M (2010a) Entrainment concepts revisited. Eur J Neurosci 25: 329-339.

Roenneberg T, Remi J, and Merrow M (2010b) Modeling a circadian surface. J Biol Rhythms 25:340-349.

Serkh K and Forger D (2014) Optimal schedules of light exposure for rapidly correcting circadian misalignment. PLoS Comput Biol 10:e1003523.

Strogatz S (1994) *Nonlinear Dynamics and Chaos: With Applications to Physics, Biology, Chemistry, and Engineering*. Reading, MA: Perseus.

Taylor S, Webb A, Smith K, Petzold L, and Doyle F (2010) Velocity response curves support the role of continuous entrainment in circadian clocks. J Biol Rhythms 25:138-149.

Taylor S, Cheever A, and Harmon S (2014) Velocity response curves demonstrate the complexity of modeling entrainable clocks. J Theor Biol 363:307-317.

Tyson J, Hong C, Thron C, and Novak B (1999) A simple model of circadian rhythms based on dimerization and proteolysis of per and tim. Biophys J 77:2411-2417.

Winfree A (2001) *The Geometry of Biological Time*. New York: Springer Science & Business Media.

Woller A, Gonze D, and Erneux T (2014) The Goodwin model revisited: Hopf bifurcation, limit-cycle, and periodic entrainment. Phys Biol 11:045002.

Wu C. and Rul'kov N (1993) Studying chaos via 1-d maps: a tutorial. IEEE Trans Circuits Syst I Fundam Theory Appl 40:707-721.

Young M (1989) The molecular control of circadian behavioral rhythms and their entrainment in drosophila. Annu Rev Biochem 67:135-152.

Supplementary Online Material — Entrainment maps: A new tool for understanding properties of circadian oscillator models

Casey O. Diekman* Amitabha Bose†

Section M1: The Entrainment Map $\Pi(x)$

Pseudocode algorithm for computing the map

Suppose the trajectory is on the Poincaré section $\mathcal{P}$ with coordinates along the LD limit cycle. Set $t = 0$ and choose $x_0 \in [0, 24)$ as the amount of time that has passed since the beginning of the most recent LD cycle, where N and $24 - N$ are the number of hours of light and dark in each LD cycle (typically $N = 12$). We wish to find $x_1 = \Pi(x_0)$, the amount of time that has passed since the beginning of the most recent LD cycle when the trajectory first returns to $\mathcal{P}$. To do this, we solve the ODEs (integrating forward in time) and record the time t when the trajectory crosses $\mathcal{P}$ according to the following algorithm:

IF $x_0 < N$

1. impose L for $N - x_0$ hours
2. then impose D for $24 - N$ hours

- **IF** trajectory reaches $\mathcal{P}$ at $t < 24 - x_0$, **THEN** set $x_1 = t + x_0$
- **ELSE** impose L for N hours
  - **IF** trajectory reaches $\mathcal{P}$ at $t < 24 - x_0 + N$, **THEN** set $x_1 = t + x_0 - 24$
  - **ELSE** impose D for $24 - N$ hours
    - **IF** trajectory reaches $\mathcal{P}$ at $t < 48 - x_0$, **THEN** set $x_1 = t + x_0 - 24$
    - **ELSE** impose L for N hours
      - **IF** trajectory reaches $\mathcal{P}$ at $t < 48 - x_0 + N$, **THEN** set $x_1 = t + x_0 - 48$

IF $x_0 \geq N$

1. impose D for $24 - x_0$ hours
2. then impose L for N hours

- **IF** trajectory reaches $\mathcal{P}$ at $t < 24 - x_0 + N$, **THEN** set $x_1 = t + x_0 - 24$
- **ELSE** impose D for $24 - N$ hours

*Department of Mathematical Sciences, New Jersey Institute of Technology, Newark, NJ 07102; diekman@njit.edu
†Department of Mathematical Sciences, New Jersey Institute of Technology, Newark, NJ 07102; bose@njit.edu

- **IF** trajectory reaches $\mathcal{P}$ at $t < 48 - x_0$ **THEN** set $x_1 = t + x_0 - 24$
- **ELSE** impose L for N hours
  - **IF** trajectory reaches $\mathcal{P}$ at $t < 48 - x_0 + N$ **THEN** set $x_1 = t + x_0 - 48$
  - **ELSE** impose D for $24 - N$ hours
    - **IF** trajectory reaches $\mathcal{P}$ at $t < 72 - x_0$ **THEN** set $x_1 = t + x_0 - 48$

The simulations were performed in MATLAB R2015a using the ODE solver *ode15s* with absolute and relative tolerances of 10^{-8}.

Section R1: Dependence of $\Pi(x)$ on parameters

Explaining how $\rho(x)$ and $\Pi(x)$ depend on ϕ

Figure S1 shows $\rho(x)$ for various values of ϕ. In general, the curves shift down and to the right as ϕ is increased. We give a simple explanation for why this occurs. Consider $\phi_1 < \phi_2$; to be definite let $\phi_1 = 2.1$ whose corresponding trajectory in phase space is already plotted in Fig. 1A of the main text. Choose the point q as the intersection point of the DD cycle with $\mathcal{N}_{P_L}$ near $P = 3.2$; see Fig. 1A. Denote the time from $\mathcal{P}$ to q along the DD cycle as x_{ϕ_1}. From the annotated phase plane shown in Fig. 1A, we note that this time is less than 12 hours. For a larger ϕ_2, because of faster dynamics the corresponding time from $\mathcal{P}$ to q (denoted x_{ϕ_2}) is smaller. Define $x_1 = 24 - x_{\phi_1}$ and $x_2 = 24 - x_{\phi_2}$. Thus $x_1 < x_2$. After the trajectories reach q, they will travel back towards $\mathcal{P}$, initially under 12 hours of light and then in darkness, if needed. Define $q(x_i)$ to be the respective times from q to $\mathcal{P}$. Note that as long as the trajectories are in the light cycle, they follow the same one-dimensional path back to P. If they both reach $\mathcal{P}$ during the L interval, then $q(x_1) > q(x_2)$ since the dynamics are slower for x_1. Omitting the details, the same conclusion will hold if one or both do not reach $\mathcal{P}$ in the L interval, but instead in the next D interval. Thus if $x_1 < x_2$, then $\rho(x_1) = x_{\phi_1} + q(x_1) > x_{\phi_2} + q(x_2) = \rho(x_2)$. Therefore the curve $\rho(x)$ shifts down and to the right. Note that x_u and x_s, which denote crossings of $\rho(x)$ with 24, occur respectively on increasing and decreasing portions of $\rho(x)$. As ϕ increases x_u moves to the right and x_s to the left. At $\phi = 2.3$, x_u passes through the boundary $x = 24$ and then, by periodicity, emerges from the $x = 0$ boundary. The points eventually merge at $\phi = 2.506$ which corresponds to ϕ_{max}. In the opposite direction, as ϕ is decreased, x_s and x_u merge when $\phi = 1.865$ which corresponds to ϕ_{min}.

The above findings lead to the following general set of properties describing how Π depends on ϕ. These properties are not unique to the NT model but also apply to the Gonze and Kim-Forger models.

(C1) There exists $\phi_{min} < \phi_{max}$ such that for any $\phi \in (\phi_{min}, \phi_{max})$, Π has a unique stable fixed point, x_s and a unique unstable fixed point, x_u. ϕ_{min} is the value of ϕ at which these fixed points are created through a saddle-node bifurcation, ϕ_{max} is where these fixed points are destroyed through a different saddle-node bifurcation.

(C2) There exists a value $\phi_c \in (\phi_{min}, \phi_{max})$, such that if $\phi \in (\phi_{min}, \phi_{max})$ and $\phi \neq \phi_c$, Π has exactly one point of discontinuity. When $\phi = \phi_c$, the map is continuous and $x_u = 0$ or equivalently 24.

(C3) If x_d is the point of discontinuity, then $\lim_{x \to x_d^-} \Pi(x) = 24$ and $\lim_{x \to x_d^+} \Pi(x) = 0$

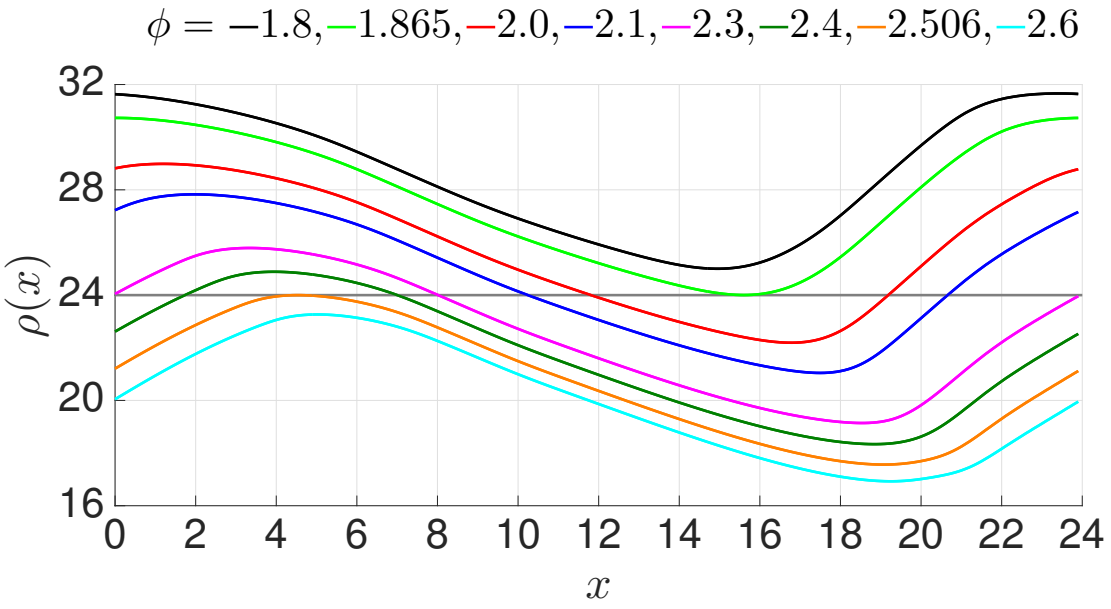

Figure S1 : The curve $\rho(x)$ shifts down and to the right as ϕ increases. When ϕ is too small or large, the curve no longer intersects $\rho = 24$ indicating loss of entrainment.

(C4) The discontinuity x_d increases as ϕ increases; it passes through the border $x = 24$ as ϕ increases through ϕ_c and then emerges from the opposite border $x = 0$.

(C5) When $\phi \neq \phi_c$, the map is periodic at the endpoints of its domain; $\Pi(0) = \Pi(24^-)$. When $\phi = \phi_c$, then $\Pi(0) = 0$, $\Pi(24^-) = 24$ and thus $\Pi(0) = \Pi(24^-) - 24$

(C6) Π is increasing on intervals where it is continuous.

The properties of $\Pi(x)$ are straightforward to understand. Note $\Pi(x_s) = \rho(x_s) + x_s$ mod 24. Since $\rho(x_s) = 24$, $\Pi(x_s) = x_s$, and similarly for x_u. Therefore C1 follows. C3 occurs whenever $\rho(x) + x$ equals a multiple of 24. Since this quantity is increasing ($\rho'(x) + 1 > 0$), the limits from above and below follow, as does C6. Properties C2, C4 and C5 are all related to how $\rho(x)$ depends on ϕ. Namely, since $\rho(x)$ moves down and to the right with increasing ϕ, the map $\Pi(x)$ must also behave similarly. This implies that the discontinuity moves to the right as ϕ increases. For large enough ϕ (fast enough oscillator), the trajectory can return to $\mathcal{P}$ within the same LD cycle as it started. In this case the discontinuity x_d occurs for small values of x and has effectively passed through the $x = 24$ border for the value ϕ_c. At that value ϕ_c, the map is continuous. The map is periodic since $\rho(x)$ is periodic and $x = 0$ is equivalent to $x = 24$.

Explaining the saddle-node bifurcation of periodic orbits

When ϕ increases through ϕ_{max} or decreases through ϕ_{min}, the fixed points x_s and x_u merge at a saddle-node bifurcation. This merging corresponds to a saddle-node bifurcation of periodic orbits in phase space as shown in Fig. S2. The dashed curves in each panel correspond to the unstable limit cycle, while the solid curves are the stable limit cycles. In each case, red denotes lights on and black lights off. The unstable limit cycle was obtained by first finding the value of x_u from the map. We then ran a direct simulation for the equivalent of one 24 hour LD cycle in which

the trajectory was started on $\mathcal{P}$ and subjected to $12 - x_u$ of light if $x_u < 12$ or $24 - x_u$ of dark if $x_u > 12$. Note that as ϕ decreases, the intrinsic oscillations of LL and DD will slow down. Thus in order to entrain, the trajectory needs to speed up as much as possible. This is why the bifurcation in phase space occurs near the LL cycle which is faster than the corresponding DD cycle; Fig. S2C. Alternatively, when ϕ increases, the intrinsic DD and LL oscillators get progressively faster. To entrain, the forced trajectory needs to be as slow as possible which is achieved nearer to the DD oscillation; Fig. S2D.

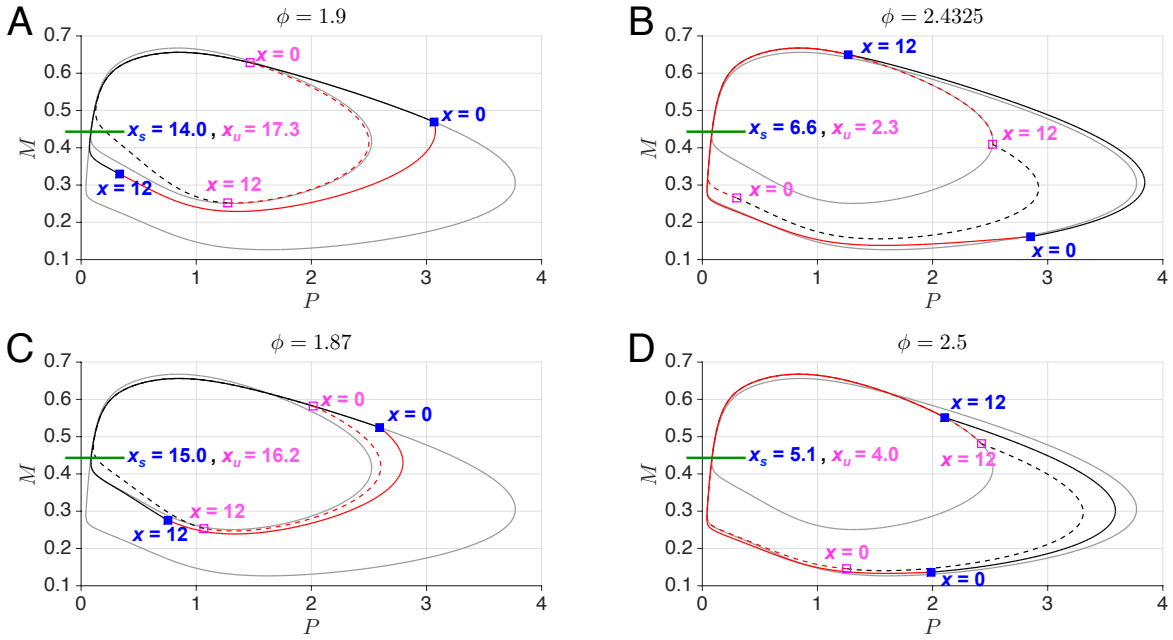

Figure S2 : Approaching saddle-node bifurcation of limit cycles as the intrinsic oscillator becomes slower (left, $\phi = 1.9$ to 1.87) or faster (right, $\phi = 2.4325$ to 2.5). The LL (inner grey) and DD (outer grey) cycles are shown in each panel. Stable limit cycles shown with solid curves , unstable ones with dashed curves. Red denotes lights on $x = 0$ to $x = 12$ and black denotes lights off $x = 12$ to $x = 0$. A. and C. As ϕ decreases, the stable and unstable limit cycles merge near the LL cycle. B. and D. As ϕ increases, those limit cycles merge near the DD cycle.

Explaining how $\Pi(x)$ depends on the photoperiod

Different parts of the map $\Pi(x)$ shift up or down depending on whether N is increased or decreased. To understand why the map behaves this way, let us first take the initial condition $x_0 = 5$ and compare in the $P - M$ phase plane the behavior of the ensuing solution trajectory for three cases, $N = 8$, 12, and 16. Consider the $N = 12$ case. Because $x_0 = 5$, the trajectory will initially experience 7 hours of light. This will place the trajectory at the point c_p (see Fig. 3A). From here, the trajectory will follow the DD cycle for 12 hours, leaving it no more than 10 hours away from $\mathcal{P}$. Indeed, from Fig. 4D, we see that $\Pi(5) \approx 8.5$. Now consider $N = 16$. Here the trajectory will initially experience 11 hours of light. That is it will travel for 4 hours more along the LL limit cycle from the point c_p than the $N = 12$ trajectory. From here the trajectory flows under dark dynamics for 8 hours. At this time, because it had a longer duration of light and a shorter duration of darkness relative to the 12:12 case, the trajectory is now closer to $\mathcal{P}$ than the $N = 12$ trajectory. As a result it should be less than 8.5 hours away, and we see that $\Pi(5) \approx 7$. Thus this portion of

Direct simulation		Entrainment map				
t	$t_{ref} - t$	x_n	x_{n+1}	$x_s - x_{n+1}$	$\rho(x_n)$	$\sum \rho(x_n)$
23.450	-9.450	20.244	19.591	-9.347	23.347	23.347
45.165	-8.165	19.591	18.193	-7.949	22.601	45.949
67.465	-5.465	18.193	15.389	-5.145	21.197	67.145
88.888	-2.888	15.389	12.932	-2.688	21.543	88.688
111.380	-1.380	12.932	11.504	-1.260	22.572	111.260
134.631	-0.631	11.504	10.819	-0.572	23.312	134.572
158.281*	-0.281	10.819	10.491	-0.247	23.676	158.247**

Table S1 : Time to reach stable entrained solution ($x_s = 10.244$) calculated by direct simulation* and by iterating the map** from initial condition $x_0 = 20.244$. For this case the oscillator entrains through phase advances as can be seen by noting the negative sign of the difference $x_s - x_{n+1}$.

the map has in fact shifted down for increased N. Next, let us consider the case of $N = 8$ with $x_0 = 5$. Now the trajectory initially gets only 3 hours of light and then must experience 16 hours of darkness. Since the time $x_D = 6.3$ (see Fig. 3A), the trajectory needs roughly 3.3 more hours to reach c_p. From there it still has 12.7 hours to travel on DD. Note that the $N = 12$ trajectory had to travel for 12 hours on DD from the point c_p. So the value of $\Pi(5)$ for the $N = 8$ photoperiod will be just smaller than that value for $N = 12$. This is again confirmed by inspection of Fig. 4D which shows that $\Pi(5) \approx 8$ for $N = 8$. Therefore this portion of the map does not shift in a stereotypical way. A similar argument using $x_0 = 17.7$ explains why the right part of the map shifts up for decreasing N, but does not shift much, if at all, for increasing N.

Section R2: Computations using entrainment maps

Dynamics of Entrainment

The map can be used to easily calculate entrainment time. An iterate landing on a particular branch (upper or lower) corresponds to a certain amount of time $\rho(x)$. This depends on the location of the discontinuity x_d. In particular, if $x_d < 12$,

$$\rho(x_{n+1}) = \begin{cases} x_{n+1} - x_n & \text{iterate lies on upper branch} \\ x_{n+1} - x_n + 24 & \text{iterate lies on lower branch,} \end{cases} \tag{1}$$

whereas if $x_d > 12$

$$\rho(x_{n+1}) = \begin{cases} x_{n+1} - x_n + 24 & \text{iterate lies on upper branch} \\ x_{n+1} - x_n + 48 & \text{iterate lies on lower branch.} \end{cases} \tag{2}$$

For example, to calculate the entrainment times shown in Fig. 5 with $x_0 = 20.244$, note that $x_u = 20.5$, $x_s = 20.244$, all iterates hit the upper branch, and $x_d > 12$, so equation (2) implies that $\rho(x_{n+1}) = x_{n+1} - x_n + 24$. We compute the values x_j for integer $j \geq 1$ by iterating the map numerically. First, we construct the map $\Pi(x)$ for a grid of evenly spaced points $x = 0, 0.1, 0.2, \ldots, 24$ through direct simulations as described in Supplementary Material Section M1. To obtain values of $\Pi(x)$ for x values that are not grid points, we simply round x to the nearest grid point value. If more accurate entrainment time estimates are needed then the map can be computed over a more finely spaced grid of x values. We find that the total time to entrainment

Direct simulation		Entrainment map				
t	$t_{ref} - t$	x_n	x_{n+1}	$x_s - x_{n+1}$	$\rho(x_n)$	$\sum \rho(x_n)$
24.734	12.266	21.244	21.882	-11.638	24.638	24.638
50.268	10.732	21.819	23.355	-13.111	25.473	50.111
77.131	7.869	23.355	2.176	8.068	26.821	76.932
104.943	4.057	2.176	6.023	4.222	27.847	104.779
131.526	1.474	6.024	8.685	1.559	26.663	131.441
156.435	0.565	8.685	9.655	0.589	24.970	156.411
180.767*	0.233	9.655	10.019	0.225	24.364	180.775**

Table S2 : Time to reach stable entrained solution ($x_s = 10.244$) calculated by direct simulation* and by iterating the map** from initial condition $x_0 = 21.244$. For this case the oscillator entrains through phase delays, as can be seen by noting the positive sign of the difference $x_s - x_{n+1}$.

is 158.247 hours (6.6 days); see Table S1. To compare with direct simulations, start with an initial condition on $\mathcal{P}$ subjected to 3.8 hours of darkness. From this point forward, we subject the perturbed oscillator to 12:12 LD and keep track of the times at which it hits the section as t_j for integer $j \geq 1$. Concurrently, we also keep track of the times at which an entrained reference oscillator would hit $\mathcal{P}$ as $t_{ref_j} = t_{ref_0} + 24(j-1)$, where the first crossing of the reference oscillator is given by t_{ref_0}. This value is calculated on a case-by-case basis. Namely, for $x_d < 12$, if $x_0 < x_u$, then $t_{ref_0} = -x_0 + x_s$. Whereas if $x_0 > x_u$, then $t_{ref_0} = 24 - x_0 + x_s$. For $x_d > 12$ if $x_0 < x_u$, then $t_{ref_0} = 24 - x_0 + x_s$. Whereas if $x_0 > x_u$, then $t_{ref_0} = 48 - x_0 + x_s$. When the magnitude of the time difference between the section crossings of the perturbed and reference oscillators is less than 0.5 hours, we consider the oscillator to be entrained. Table S3 shows results when $x_0 = 21.244$ which is the to right of x_u. From the map, we find entrainment time to be 180.775 hours (7.5 days) and from direct simulations 180.767 hours.

Comparison to results using a different Poincaré section

Choose a new Poincaré section, $\mathcal{P}_*$, at $M = 0.44$, $dM/dt < 0$ which is near the maximum value of P along the LD-entrained solution. The section $\mathcal{P}_*$ is located 9.669 hours later along the LD-entrained solution than the section $\mathcal{P}$ chosen in the main text. Fig. S3A shows the entrainment maps for $\mathcal{P}$ and $\mathcal{P}_*$. Note that the stable fixed point of the new map is $x_s = 19.913$, which is exactly 9.669 hours later than the value 10.244, which was the fixed point of the original map. Thus, as must be the case, the phase relationship between the light-dark cycle and the LD-entrained solution is the same independent of the Poincaré section that is chosen. What will differ is the time to entrainment for initial conditions associated with either map. This is because an initial condition x_0 chosen for the maps corresponds to an initial condition lying on $\mathcal{P}$ for the original map and $\mathcal{P}_*$ for the new one. These points lie in different regions of the (P, M) phase space and would therefore not be expected to have similar entrainment times as shown in Fig. S3B. For example, consider $x_0 = 12$, which corresponds to the transition from light to dark in a 12:12 LD cycle. A trajectory starting at $\mathcal{P}$ entrains relatively quickly (46.63 hours) through phase advances (green cobweb in Fig. S3A), whereas a trajectory starting at $\mathcal{P}_*$ takes longer to entrain (103.69 hours) and does so through phase delays (magenta cobweb in Fig. S3A). The fact that the trajectory starting at $\mathcal{P}$ entrains more quickly is not surprising since x_0 is closer to the stable fixed point of the $\mathcal{P}$ map ($x_0 - x_s(\mathcal{P}) = 1.756$) than it is to the stable fixed point of the $\mathcal{P}_*$ map ($x_0 - x_s(\mathcal{P}_*) = -7.913$). An initial condition for the $\mathcal{P}$ map that would be equivalent to $x_0 = 12$ for the $\mathcal{P}_*$ map is one that

is 7.913 hours earlier than $x_s(\mathcal{P})$, i.e. $x_0 = 2.331$. A trajectory starting at $\mathcal{P}$ with this x_0 entrains through phase delays with the same entrainment time (103.69 hours) as does $x_0 = 12$ for the $\mathcal{P}_*$ map (cyan cobweb in Fig. S3A). In general, we can align initial conditions x_0 for different maps in the following way:

$$\hat{x} = \begin{cases} x_0 - x_s + 24 & \text{if} \quad x_0 < x_s - 12 \\ x_0 - x_s & \text{if} \quad x_0 \in [x_s - 12, x_s + 12] \\ x_0 - x_s - 24 & \text{if} \quad x_0 > x_s + 12 \end{cases} \tag{3}$$

where the normalized initial conditions $\hat{x}$ have domain $[-12, 12]$. Figure S3C shows that after alignment of initial conditions, the entrainment time curves for the two different Poincaré sections nearly overlap. This indicates that initial conditions that start with the same relative offset from the entraining light-dark cycle will have similar, but not identical, entrainment times. The entrainment times are not identical because the choice of a section specifies the phase along the LD-entrained solution at which the perturbation that the oscillator must re-entrain from occurs, and in general we would not expect the same perturbation applied at different points on the LD-entrained solution to yield exactly the same entrainment time. Figure S3D shows that all trajectories converge to the same LD-entrained solution with the same phase of entrainment regardless of where the Poincaré section is located.

Section R3: Relating $\Pi(x)$ to a PRC

Figure S4 shows the relationship between $\Pi(x)$ and $Z_1(y)$ for the case when $\tau = 24$. Table S3 shows a comparison between the predicted phase of entrainment from the map versus direct simulation. The three columns on the right show the error in minutes for the predictions provide by Π, Z_1 and Z_2. The error using the maps is negligible. The errors associated with Z_1 and Z_2 are larger, though they improve as τ increases. The reason that the prediction for Z_1 improves for larger τ is that because of the longer period, the time when the light is felt by the trajectory shifts. For example, when $\tau = 24$, the light pulse effects the solutions as the locations shown in Fig. 8. As the period increases, the location at where the trajectory experiences light shifts counterclockwise. This means that in the calculation of Z_1, increasingly more of the 12 hours of light are used. At $\tau = 29.79$, the prediction made by Z_1 is determined using 8 hours of light. The other 4 hours of light that are used by Π to determine its prediction occur in a region of phase space (near the left branch of $\mathcal{N}_P$) where the oscillator has roughly the same speed in both light and dark. Thus we expect the prediction made by Z_1 to converge to that made by Π. That Z_2 also makes a better prediction as τ increases is mostly due to the improved accuracy of Z_1. For large enough τ, there would be no light pulse during the second cycle of the oscillation and thus there would be no additional change in phase. That is for τ large enough $Z_1(y) = Z_2(y)$. Finally, we explain why Z_1 fails to make a prediction when $\tau \leq 24$. For smaller τ, the fixed point x_s is smaller (near 5), which in turn means that the corresponding value y is large (near 19). For $\tau < 24$, the PRC needs to be negative near the fixed point in order to slow the oscillation. But when y is large, the lights turn on in a region of the left branch of $\mathcal{N}_P$, where it has little effect. Thus $Z_1(y) \approx 0$ for $y > 19$ and there is no predicted fixed point.

Section R4: Higher dimensional models

Figure S5 shows the three-dimensional phase space of the Gonze model. The main point to note here is that the DD and LL limit cycles do not lie anywhere near the LD limit cycle. The entrainment

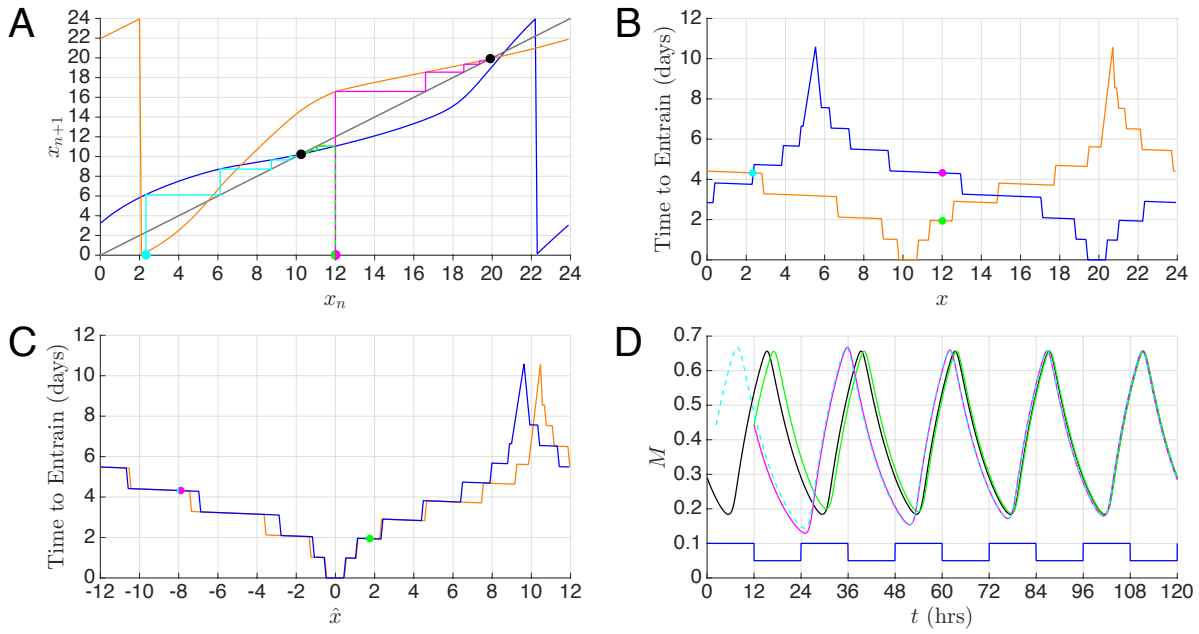

Figure S3 : Map predictions of entrainment phase and time to entrainment are consistent across different Poincaré sections. A. Entrainment map based on the original section $\mathcal{P}$ (blue) and a new section $\mathcal{P}_*$ (orange) with stable fixed points at $x_s(\mathcal{P}) = 10.244$ and $x_s(\mathcal{P}_*) = 19.913$ (solid black dots). The green and magenta orbits show iterates starting at initial condition $x_0 = 12$ for the $\mathcal{P}$ and $\mathcal{P}_*$ maps, respectively. The cyan orbit shows iterates of the $\mathcal{P}$ map starting at $x_0 = 2.331$, which is the same distance from $x_s(\mathcal{P})$ as $x_0 = 12$ is from $x_s(\mathcal{P}_*)$. B. Entrainment time curves showing that the magenta and cyan orbits, which have the same relative offset from the entraining light-dark cycle, take the same amount of time to entrain. The green orbit, which has a smaller relative offset, entrains more quickly. C. The entrainment time curves for the two different sections largely overlap after aligning initial conditions based on the relative offset from the entraining light-dark cycle. D. Time course of M variable showing that trajectories starting at different Poincaré sections converge to the same LD-entrained solution. The green and magenta solutions start with $x_0 = 12$ on $\mathcal{P}$ and $\mathcal{P}_*$ respectively, and the cyan solution starts on $\mathcal{P}$ with $x_0 = 2.331$ (time traces for each case begin with appropriate offset from the start of the LD cycle). The solid black trace is the reference solution entrained to the LD forcing shown below in blue. Note that the magenta and cyan solutions have very similar times to entrainment, through phase delay, as predicted by the map.

map uses a Poincaré section along the LD trajectory as shown, whereas the PRC would perturb off of the DD cycle. The ensuing trajectories should therefore be expected to provide different phase-resetting predictions.

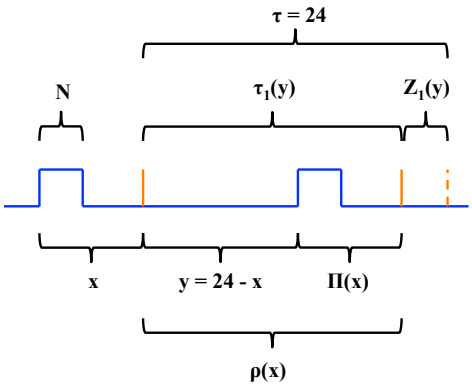

Figure S4 : Schematic showing the relationship between $\pi(x)$, $\rho(x)$, and the PRC for the case $\tau = 24$. Solid red lines depict where in time the oscillator crosses the Poincaré section $\mathcal{P}$. Dashed line is the location in time where the reference oscillator crosses the section.

		Predicted phase of entrainment				Error (minutes)		
ϕ	τ	Direct simulation	Entrainment map Π	PRC Z_1	PRC Z_2	Π	Z_1	Z_2
8.25	23.5	4.711	4.709	-	5.354	0.12	-	38.6
8.15	23.8	5.250	5.250	-	5.936	0.04	-	41.1
8.07	24.0	5.478	5.479	-	6.189	0.02	-	42.7
8	24.2	5.644	5.644	5.166	6.373	0.02	28.7	43.7
7.5	25.8	6.588	6.588	6.349	7.393	0.01	14.3	48.3
7	27.7	7.455	7.455	7.269	8.120	0.01	11.2	39.9
6.5	29.8	8.388	8.388	8.320	8.588	0.00	4.1	12.0
6	32.3	9.757	9.757	9.756	9.757	0.01	0.01	0.04
5.5	35.2	12.424	12.424	12.424	12.424	0.01	0.01	0.01

Table S3 : Comparison of entrainment map and PRC accuracy in predicting phase of entrainment for a range of τ values with $\epsilon = 0.01$. In all cases, the entrainment map makes accurate predictions, while those made by the PRCs are inaccurate (except for larger values of τ as explained in the text.)

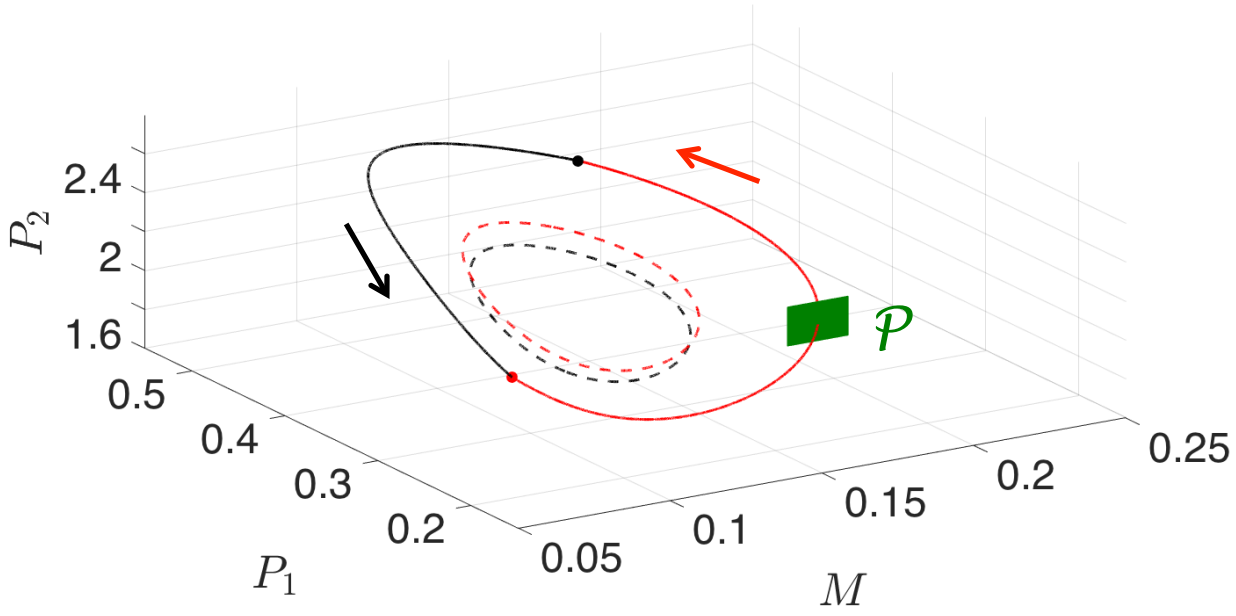

Figure S5 : Limit cycles of the Gonze model. DD (dashed black), LL (dashed red), and LD (solid red/black) trajectories in the three-dimensional phase space. A patch of the Poincaré section $\mathcal{P}$ (a two-dimensional hyperplane) is shown in green, defined as $P_1 = 0.35$ with P increasing.